NASA Technical Memorandum 74065

(NASA-TM-74065) INVESTIGATION OF SUPERSONIC TURBULENT BOUNDARY-LAYER SEPARATION ON A COMPRESSION RAMP BY AN INTEGRAL METHOD (NASA) 62 p HC A04/MF A01 CSCL 20D

N77-33439

Unclas
G3/34 49413

INVESTIGATION OF SUPERSONIC TURBULENT BOUNDARY-LAYER SEPARATION ON A COMPRESSION RAMP BY AN INTEGRAL METHOD

D. K. Patel and K. R. Czarnecki

October 1977

National Aeronautics and Space Administration

Langley Research Center
Hampton, Virginia 23665

ORIGINAL PAGE IS
OF POOR QUALITY

INVESTIGATION OF SUPERSONIC TURBULENT BOUNDARY-LAYER SEPARATION ON A COMPRESSION RAMP BY AN INTEGRAL METHOD

D. K. Patel and K. R. Czarnecki

SUMMARY

An investigation was made to determine the feasibility of using a boundary-layer integral method to study the separation of a turbulent boundary layer on a two-dimensional ramp at supersonic speeds. The numerical calculations were made for a free-stream Mach number of 3, a Reynolds number of 10 million, and over a ramp-angle range from 0° to 30°.

For ramp angles where no flow separation was indicated, the theoretical calculations were in reasonable agreement with experimental data except for a somewhat belated rise in the pressure. For the larger ramp angles, where separation was present, the investigation produced results that were not in agreement with experiment or with results calculated by time-dependent Navier-Stokes methods apparently because no provision had been made for a proper shock-boundary layer interaction where strong normal pressure gradients are induced within the boundary layer under the shock independent of surface curvature effects. Within the limits of the calculations, the effects of changes in the size of the fillet, the omission of curvature terms, and changes in eddy-viscosity model were negligible.

INTRODUCTION

With the development of large high-speed computers, one of the aerodynamic problems currently receiving considerable theoretical attention is that of the separation of a turbulent boundary layer in a two-dimensional compression corner at supersonic and hypersonic speeds.

Although progress is being made in theoretically predicting separation characteristics which agree reasonably well with experiment (see refs. 1 and 2) many aspects of the problem remain unsolved. In particular, for combinations of free-stream Mach number and ramp angle for which there is no shock detachment in inviscid flow and if the boundary-layer thickness is small relative to ramp chord the length of the separation region is dependent upon boundary characteristics alone. For combinations of Mach number and ramp angle which result in the shock detachment angles being exceeded the separation length is dependent primarily upon the maximum height of the ramp if the boundary layer is relatively thin and on both the ramp height and boundary-layer characteristics if the boundary layer is relatively thick, in close analogy to the forward-facing step flow separation (ref. 3). The transition from one regime to the other needs further investigation. This investigation can best be done by a parametric study. Unfortunately, the time-dependent Navier-Stokes methods which appear to give reasonable results (refs. 1 and 2) are rather expensive and lengthy timewise for such an investigation. Consequently, it appeared desirable to determine if it was feasible to make such a study using a boundary-layer integral method where the inherent simplifying assumptions generally eliminate significant amounts of computer time.

The boundary-layer integral method used in this investigation is based on the method devised by Kuhn and Nielson (refs. 4 and 5) and extended by Tai to include the strong-interaction case (ref. 6). The same velocity profiles and eddy-viscosity models utilized by the aforementioned investigators were used, but the basic boundary-layer equations were modified to include surface curvature terms so that a singularity at the intersection of the ramp with the flat plate could be eliminated by incorporating a fillet. External-flow characteristics were determined assuming a Prandtl-Meyer supersonic flow. No investigation was made of the case where the external flow behind the boundary-layer reattachment point was subsonic or of the characteristics of separated-flow regions because of a major deficiency in the general method. Both the weak- and strong-interaction methods of Tai were investigated along with many modifications.

ORIGINAL PAGE IS
OF POOR QUALITY

ORIGINAL PAGE IS
OF POOR QUALITY

Numerical calculations were made for a free-stream Mach number of 3, over a ramp angle range from 0° to 30°, at a Reynolds number, based on the flat-plate length to the ramp leading edge, of 10 million. The fillet between the ramp and flat plate was varied from 1.5 to 6 percent of the flat-plate length to the ramp and its shape was varied. Most of the solutions were obtained by a point-iteration downstream-marching procedure but some global iteration solutions were also obtained for comparison.

NOMENCLATURE

a	speed of sound
c_f	local skin-friction coefficient, $\dfrac{\hat{\tau}_w}{1/2\hat{\rho}_\infty \hat{u}_\infty^2}$
c_i	coefficients of polynomial, equation A-1
D	distance from plate-ramp corner to beginning or end of fillet, figure 10
E_{ij}	functions defined in equations C-1 through C-9
$f(n)$	weighting function, equation 22
$F(n)$	function defined in equation C-13
k	constant in equation 35
$\hat{\ell}$	distance from leading edge of flat plate to plate-ramp corner
m	constant in equations 34 and 35
M	Mach number
n^+	dimensionless normal distance from plate-ramp surface, $\dfrac{\lvert\hat{u}_\tau\rvert\hat{n}}{\hat{\nu}}$

N	exponential constant in equation 3
p	dimensionless static pressure $\frac{\hat{p}}{\hat{p}_\infty}$
Q_j	functions defined in equations C-10 through C-12
r	dimensionless radius of curvature, $\frac{\hat{r}}{\hat{\ell}}$
R_∞	Reynolds number, $\frac{\hat{\rho}_\infty \hat{u}_\infty \hat{\ell}}{\hat{\mu}_\infty}$
s,n	dimensionless orthogonal curvilinear coordinates measured along and normal to plate-ramp surface; $\frac{\hat{s}}{\hat{\ell}}$, $\frac{\hat{n}}{\hat{\ell}}$
$\hat{t}$	time
T	dimensionless temperature, $\frac{\hat{T}}{\hat{T}_\infty}$
u,v	dimensionless velocity components along and normal to plate-ramp surface; $\frac{\hat{u}}{\hat{u}_\infty}$, $\frac{\hat{v}}{\hat{u}_\infty}$
u_β	dimensionless wake velocity, $\frac{\hat{u}_\beta}{\hat{u}_\infty}$
u_τ	dimensionless friction velocity, $\frac{\hat{u}_\tau}{\hat{u}_\infty}$
$\hat{u}_\tau$	friction velocity, $\sqrt{\frac{\hat{\tau}_w}{\hat{\rho}_\infty}}$
V	dimensionless resultant velocity, $\sqrt{u_e^2 + v_e^2}$
x,y	cartesian coordinates

ORIGINAL PAGE IS
OF POOR QUALITY

ORIGINAL PAGE IS
OF POOR QUALITY

α	ramp angle
β	eddy viscosity, defined in equations 27-30
β^*	function defined in equation 3
β_1,β_2,β_3	eddy-viscosity parameters, equation 19
γ	specific-heat ratio
δ	dimensionless boundary-layer total thickness, $\frac{\hat{\delta}}{\hat{\ell}}$
δ^*	dimensionless boundary-layer displacement thickness $\frac{\hat{\delta}^*}{\hat{\ell}}$
$\hat{\varepsilon}$	eddy viscosity
θ	dimensionless boundary-layer momentum thickness $\frac{\hat{\theta}}{\hat{\ell}}$
Θ	boundary-layer flow angle defined by equation 38 or equation 41
λ	exponent denoting temperature-viscosity relationship, equation 3
$\hat{\mu}$	viscosity
ν	Prandtl-Meyer angle
$\hat{\nu}$	kinematic viscosity
$\hat{\rho}$	density
σ	exponent defined in equation 22
τ	dimensionless shear stress, $\frac{\hat{\tau}}{\hat{\rho}_\infty \hat{u}_\infty^2}$

Subscripts

c	compressible flow
e	edge of boundary layer

m	median
t	total or stagnation
w	wall
∞	free-stream

Superscripts

'	turbulent fluctuating velocities
-	time averaged mean quantities
^	dimensional quantities

Note: All quantities without the subscript c are in the incompressible-flow plane.

THEORETICAL MODEL

Details of the theoretical model used in this investigation are shown in figure 1. A two-dimensional supersonic turbulent boundary layer on a flat plate approaches and then is deflected onto the ramp surface at corner C. If the ramp angle is sufficiently small the boundary layer remains attached during the turn and ensuing encounter with a strong adverse pressure gradient. In order to eliminate a singularity in the computations a fillet is incorporated into the corner, the size and shape of which can be varied to influence the shape of the pressure rise if necessary. (For details of fillet design see Appendix A.) Thus, the usual thin corner shock is essentially replaced by a set of strong coalescing compression waves and the expected abrupt pressure jump by a steep but finite adverse pressure gradient. Inasmuch as boundary-layer separation might be expected to first occur on the fillet as the ramp angle is sufficiently increased this approach requires that the basic boundary-layer equations retain curvature terms to $r \sim O(\delta)$. The inviscid flow

ORIGINAL PAGE IS
OF POOR QUALITY

ORIGINAL PAGE IS
OF POOR QUALITY

above the boundary layer was assumed to be governed by the Prandtl-Meyer relations. Calculations indicated that the maximum expected entropy changes should be small and their influence on the flow characteristics negligible for the range of conditions that were to be explored in this investigation.

For greater simplicity the viscous boundary-layer calculations were made in the constant property or incompressible-flow plane with the transition from or to the compressible boundary layer being made via Stewartson's transformation (ref. 7). The interaction between the boundary layer and inviscid exterior flow was investigated in the compressible-flow plane by two methods. In the weak interaction (see ref. 6) the angle of the inviscid stream was matched to the angle generated by the growth of the displacement thickness of the boundary layer and the velocity at the edge of the boundary layer was then matched to that of the stream. In the strong interaction the velocity and flow angle of the inviscid flow were matched to the velocity and streamline angle at the edge of the boundary layer.

INVISCID FLOW

The pressure, density, Mach number, etc., characteristics of the inviscid flow over the boundary layer were determined by Prandtl-Meyer flow. Preliminary calculations based on experimental indications revealed that the entropy changes that might occur in actual physical flows were relatively small for the Mach number range of the investigation and that their omission in the present theoretical approach would have no significant effect on the general flow characteristics to be calculated. Actually, the calculations were made by using the Prandtl-Meyer flow tables of NACA 1135 (ref. 8) with the Prandtl-Meyer angle ν being used as the entering variable to make the interpolations. The angle ν is found from either the slope of the boundary-layer displacement thickness or the angle of the flow at the outer edge of the boundary layer in the compressible-flow plane.

VISCOUS FLOW

Stewartson Transformation

As mentioned earlier the boundary-layer calculations were made in the incompressible-flow plane whereas the interaction between the inviscid and viscous flows were carried out in the compressible-flow plane. The transformation from one plane to the other was accomplished by means of the Stewartson transformation (ref. 7).

$$
\left.
\begin{aligned}
\hat{s} &= \int_0^{\hat{s}_c} \frac{\hat{p}_{e,c}}{\hat{p}_{\infty,c}} \frac{\hat{a}_{e,c}}{\hat{a}_{\infty,c}} \, d\hat{\xi}_c \\
\hat{n} &= \int_0^{\hat{n}_c} \frac{\hat{\rho}_{e,c}}{\hat{\rho}_{\infty,c}} \frac{\hat{a}_{e,c}}{\hat{a}_{\infty,c}} \frac{\hat{\rho}_c}{\hat{\rho}_{e,c}} \, d\hat{\eta}_c \\
\hat{u} &= \frac{\hat{a}_{e,c}}{\hat{a}_{\infty,c}} \hat{u}_c \\
\hat{v} &= \frac{\hat{\rho}_{\infty,c}}{\hat{\rho}_{e,c}} \frac{\hat{a}_{\infty,c}}{\hat{a}_{e,c}} \left(\frac{\hat{\rho}_c}{\hat{\rho}_{\infty,c}} \hat{v}_c + \hat{u}_c \frac{\hat{a}_{\infty,c}}{\hat{a}_{e,c}} \frac{\partial}{\partial \hat{s}_c} \int_0^{\hat{n}_c} \frac{\hat{a}_{e,c}}{\hat{a}_{\infty,c}} \frac{\hat{\rho}_c}{\hat{\rho}_{e,c}} \, d\hat{\eta}_c \right)
\end{aligned}
\right\} \quad (1)
$$

Additional transformation equations can be derived directly from the definitions of the pertinent quantities and the Stewartson transformation or from the definitions, transformation and Crocco's relationship between

ORIGINAL PAGE IS
OE POOR QUALITY

ORIGINAL PAGE IS
OF POOR QUALITY

local temperatures and velocities within a boundary layer having a constant static pressure and total temperature across the layer. Some of the more useful relationships are

$$\left.\begin{aligned}
\hat{\delta}_c &= \hat{\delta}\left[\frac{\hat{T}_t}{\hat{T}_e} - \frac{\gamma - 1}{2} M_e^2 \int_0^{\hat{\delta}} \left(\frac{\hat{u}}{\hat{u}_e}\right)^2 d\hat{n}\right] \Bigg/ \left(\frac{\hat{a}_{e,c}}{\hat{a}_{\infty,c}} \frac{\hat{\rho}_{e,c}}{\hat{\rho}_{\infty,c}}\right) \\
\hat{\delta}_c^* &= \frac{\hat{\delta}^* \frac{\hat{T}_{w,c}}{\hat{T}_{e,c}} + \frac{\gamma - 1}{2} M_{e,c}^2 \hat{\theta}}{\frac{\hat{a}_{e,c}}{\hat{a}_{\infty,c}} \frac{\hat{\rho}_{e,c}}{\hat{\rho}_{\infty,c}}} \\
\hat{\theta}_c &= \frac{\hat{\theta}}{\frac{\hat{a}_{e,c}}{\hat{a}_{\infty,c}} \frac{\hat{\rho}_{e,c}}{\hat{\rho}_{\infty,c}}}
\end{aligned}\right\} \qquad (2)$$

The transformation equation derived from the Stewartson transformation for the local skin-friction coefficients was not considered reliable because it depended upon the temperatures or densities at the wall whereas the T' methods indicate a mean boundary-layer temperature or density approach is more reliable. (See ref. 9, for example.) For this investigation therefore the assumption was made for simplicity that such an equation derived in reference 10 would be adequate

$$\frac{c_{f,c}}{c_f} = \beta^*(1 - (1 + \lambda)\, N) \tag{3}$$

where

$$\beta^* = \left(1 + \frac{\gamma + 1}{4} M^2_{e,c}\right)^{-1}$$

$$\lambda = 0.76$$

$$N = \frac{1}{7}$$

Governing Equations

The basic boundary-layer equations were derived from the two-dimensional incompressible Navier-Stokes equations in the curvilinear orthogonal coordinate system (ref. 11, page 98):

Continuity

$$\frac{\hat{r}}{\hat{r} + \hat{n}} \frac{\partial \hat{u}}{\partial \hat{s}} + \frac{\partial \hat{v}}{\partial \hat{n}} + \frac{\hat{v}}{\hat{r} + \hat{n}} = 0 \tag{4}$$

$\hat{s}$-Momentum

$$\frac{\partial \hat{u}}{\partial \hat{t}} + \frac{\hat{r}}{\hat{r} + \hat{n}} \frac{\partial \hat{u}}{\partial \hat{s}} \hat{u} + \hat{v} \frac{\partial \hat{u}}{\partial \hat{n}} + \frac{\hat{v}\hat{u}}{\hat{r} + \hat{n}} = - \frac{\hat{r}}{\hat{r} + \hat{n}} \frac{1}{\hat{\rho}} \frac{\partial \hat{p}}{\partial \hat{s}}$$

$$+ \hat{\nu} \left[\frac{\hat{r}^2}{(\hat{r} + \hat{n})^2} \frac{\partial^2 \hat{u}}{\partial \hat{s}^2} + \frac{\partial^2 \hat{u}}{\partial \hat{n}^2} + \frac{1}{\hat{r} + \hat{n}} \frac{\partial \hat{u}}{\partial \hat{n}} - \frac{\hat{u}}{(\hat{r} + \hat{n})^2} \right.$$

$$\left. + \frac{2\hat{r}}{(\hat{r} + \hat{n})^2} \frac{\partial \hat{v}}{\partial \hat{s}} - \frac{\hat{r}}{(\hat{r} + \hat{n})^3} \frac{\partial \hat{r}}{\partial \hat{s}} \hat{v} + \frac{\hat{r}\,\hat{n}}{(\hat{r} + \hat{n})^3} \frac{\partial \hat{r}}{\partial \hat{s}} \frac{\partial \hat{u}}{\partial \hat{s}} \right] \tag{5}$$

ORIGINAL PAGE IS
OF POOR QUALITY

ORIGINAL PAGE IS
OF POOR QUALITY

$\hat{n}$-Momentum

$$\frac{\partial \hat{v}}{\partial \hat{t}} + \frac{\hat{r}}{\hat{r}+\hat{n}}\hat{u}\frac{\partial \hat{v}}{\partial \hat{s}} + \hat{v}\frac{\partial \hat{v}}{\partial \hat{n}} - \frac{\hat{u}^2}{\hat{r}+\hat{n}} = -\frac{1}{\hat{\rho}}\frac{\partial \hat{p}}{\partial \hat{n}}$$

$$+ \hat{\nu}\left[\frac{\partial^2 \hat{v}}{\partial \hat{n}^2} - \frac{2\hat{r}}{(\hat{r}+\hat{n})^2}\frac{\partial \hat{u}}{\partial \hat{s}} + \frac{1}{\hat{r}+\hat{n}}\frac{\partial \hat{v}}{\partial \hat{n}} + \frac{\hat{r}^2}{(\hat{r}+\hat{n})^2}\frac{\partial^2 \hat{v}}{\partial \hat{s}^2}\right.$$

$$\left. - \frac{\hat{v}}{(\hat{r}+\hat{n})^2} + \frac{\hat{r}}{(\hat{r}+\hat{n})^3}\frac{\partial \hat{r}}{\partial \hat{s}}\hat{u} + \frac{\hat{r}\,\hat{n}}{(\hat{r}+\hat{n})^3}\frac{\partial \hat{r}}{\partial \hat{s}}\frac{\partial \hat{v}}{\partial \hat{s}}\right] \qquad (6)$$

In the analysis the steady-state case is considered, thus, the $\frac{\partial}{\partial \hat{t}}$ terms become zero in equations (5) and (6).

To convert the above equations to dimensionless form the following dimensionless ratios were adopted

$$s = \frac{\hat{s}}{\hat{\ell}} \qquad u = \frac{\hat{u}}{\hat{u}_\infty} \qquad p = \frac{\hat{p}}{\hat{\rho}_\infty \hat{u}_\infty^2}$$

$$n = \frac{\hat{n}}{\hat{\ell}} \qquad v = \frac{\hat{v}}{\hat{u}_\infty} \qquad R_\infty = \frac{\hat{u}_\infty \hat{\ell}}{\hat{\nu}}$$

$$r = \frac{\hat{r}}{\hat{\ell}}$$

Here $\hat{\rho} = \hat{\rho}_\infty$ for incompressible flow. $\hat{\ell}$ is the distance between the flat-plate leading edge and the ramp corner.

Thus, equations (4) through (6) become:

$$\frac{r}{r+n}\frac{\partial u}{\partial s} + \frac{\partial v}{\partial n} + \frac{v}{r+n} = 0 \qquad (7)$$

$$\frac{r}{r+n}\,u\,\frac{\partial u}{\partial s} + v\,\frac{\partial u}{\partial n} + \frac{v\,u}{r+n} = -\frac{r}{r+n}\,\frac{\partial p}{\partial s}$$

$$+\frac{1}{R_\infty}\left[\frac{r^2}{(r+n)^2}\,\frac{\partial^2 u}{\partial s^2} + \frac{\partial^2 u}{\partial n^2} + \frac{1}{r+n}\,\frac{\partial u}{\partial n} - \frac{u}{(r+n)^2}\right.$$

$$\left.+\frac{2r}{(r+n)^2}\,\frac{\partial v}{\partial s} - \frac{r}{(r+n)^3}\,\frac{\partial r}{\partial s}\,v + \frac{r\,n}{(r+n)^3}\,\frac{\partial r}{\partial s}\,\frac{\partial u}{\partial s}\right] \qquad (8)$$

$$\frac{r}{r+n}\,u\,\frac{\partial v}{\partial s} + v\,\frac{\partial v}{\partial n} - \frac{u^2}{r+n} = -\frac{\partial p}{\partial n} + \frac{1}{R_\infty}\left[\frac{\partial^2 v}{\partial n^2}\right.$$

$$-\frac{2r}{(r+n)^2}\,\frac{\partial u}{\partial s} + \frac{1}{r+n}\,\frac{\partial v}{\partial n} + \frac{r^2}{(r+n)^2}\,\frac{\partial^2 v}{\partial s^2} - \frac{v}{(r+n)^2}$$

$$\left.+\frac{r}{(r+n)^3}\,\frac{\partial r}{\partial s}\,u + \frac{r\,n}{(r+n)^3}\,\frac{\partial r}{\partial s}\,\frac{\partial v}{\partial s}\right] \qquad (9)$$

Equations (7) through (9) are reduced to boundary-layer equations by the standard order of magnitude analysis used for shockless boundary layers. This procedure does not take into account that under the shock the $\frac{\partial}{\partial s}$ terms are on the same order of magnitude as the $\frac{\partial}{\partial n}$ terms and, consequently, large normal pressure gradients may be induced by terms other than those involving centrifugal forces. In particular, the $n\frac{\partial v}{\partial s}$ term is probably very important in generating normal pressure gradients and having a strong influence on the boundary-layer separation characteristics under a shock. Still, it is of interest to determine whether the significant characteristics

ORIGINAL PAGE IS
OF POOR QUALITY

ORIGINAL PAGE IS
OF POOR QUALITY

of the separation can be reproduced by inducing separation by means of the adverse gradients generated by a fillet and making the calculations by means of a second-order boundary-layer theory. Experimental results indicate that the pressure rises associated with shock-induced separation occur in one or two boundary-layer thicknesses (see ref. 12, for example); thus, the fillet must be relatively small. Estimates indicate that curvature terms of $r = O(\delta)$ must be retained in the equations. The results are:

Continuity:

$$\frac{r}{r+n}\frac{\partial u}{\partial s} + \frac{\partial v}{\partial n} + \frac{v}{r+n} = 0 \tag{10}$$

s-Momentum:

$$\frac{r}{r+n}u\frac{\partial u}{\partial s} + v\frac{\partial u}{\partial n} + \frac{uv}{r+n} = -\frac{r}{r+n}\frac{\partial p}{\partial s}$$

$$+ \frac{1}{R_\infty}\left[\frac{\partial^2 u}{\partial n^2} + \frac{1}{r+n}\frac{\partial u}{\partial n} - \frac{u}{(r+n)^2}\right] \tag{11}$$

n-Momentum:

$$\frac{\partial p}{\partial n} = \frac{u^2}{r+n} \tag{12}$$

To convert the equations (10) through (12) to turbulent-flow equations, let

$$u = \bar{u} + u'$$

$$v = \bar{v} + v'$$

$$p = \bar{p} + p'$$

and after substitution of the above values in equations (10) through (12) and after the equations are mean time averaged, the following equations are obtained

$$\frac{r}{r+n}\frac{\partial \bar{u}}{\partial s} + \frac{\partial \bar{v}}{\partial n} + \frac{\bar{v}}{r+n} = 0 \tag{13}$$

$$\frac{r}{r+n}\bar{u}\frac{\partial \bar{u}}{\partial s} + \bar{v}\frac{\partial \bar{u}}{\partial n} + \frac{\bar{u}\bar{v}}{r+n} = -\frac{r}{r+n}\frac{\partial \bar{p}}{\partial s} + \frac{1}{R_\infty}\left[\frac{\partial^2 \bar{u}}{\partial n^2} + \frac{1}{r+n}\frac{\partial u}{\partial n} - \frac{\bar{u}}{(r+n)^2}\right] - \frac{r}{(r+n)}\frac{\partial}{\partial s}\left(\overline{u'^2}\right) - \frac{\partial}{\partial n}\left(\overline{u'v'}\right) - \frac{2\overline{u'v'}}{r+n} \tag{14}$$

$$\frac{\partial \bar{p}}{\partial n} = \frac{\bar{u}^2}{r+n} + \frac{\overline{u'^2}}{r+n} \tag{15}$$

In the shock interaction region the magnitude and characteristics of the term $\overline{u'^2}$ is not well known (ref. 13). Thus, for this analysis the term $\overline{u'^2}$ is not taken into account.

In order to eliminate the Reynolds shear stress, an eddy viscosity is introduced as

$$-\overline{u'v'} = \frac{1}{R_\infty}\frac{\hat{\varepsilon}}{\hat{\mu}}\frac{\partial \bar{u}}{\partial n} \tag{16}$$

ORIGINAL PAGE IS
OE POOR QUALITY

ORIGINAL PAGE IS
OF POOR QUALITY

Thus, equations (14) and (15) become

s-Momentum:

$$\frac{r}{r+n}\bar{u}\frac{\partial\bar{u}}{\partial s}+\bar{v}\frac{\partial\bar{u}}{\partial n}+\frac{\bar{u}\bar{v}}{r+n}=-\frac{r}{r+n}\frac{\partial\bar{p}}{\partial s}$$

$$+\frac{1}{R_\infty}\left[\frac{\partial}{\partial n}\left(\beta_1\frac{\partial\bar{u}}{\partial n}\right)+\frac{1}{r+n}\beta_2\frac{\partial\bar{u}}{\partial n}-\frac{\beta_3\bar{u}}{(r+n)^2}\right] \tag{17}$$

and

n-Momentum:

$$\frac{\partial\bar{p}}{\partial n}=\frac{\bar{u}^2}{r+n} \tag{18}$$

where

$$\left.\begin{aligned}\beta_1&=1+\frac{\hat{\varepsilon}}{\hat{\mu}}\\ \beta_2&=1+\frac{2\hat{\varepsilon}}{\hat{\mu}}=2\beta_1-1\\ \beta_3&=1\end{aligned}\right\} \tag{19}$$

Equations (13), (17), and (18) are the governing equations for the viscous flow. The boundary conditions are $\bar{u}=o$, $\bar{v}=\bar{v}_w$ at the surface and $\bar{u}=\bar{u}_e(s)$ at the edge of the boundary layer for the weak interaction and $\bar{u}=o$, $\bar{v}=\bar{v}_w$

at the surface and $V(s) = \sqrt{u_e^2 + v_e^2}$ at the edge of the boundary layer for the strong interaction. $\bar{v}_w$ represents a surface injection or suction velocity if one is desired.

Integral Method

The desired integral equation is obtained by combining the continuity, s- and n-momentum equations (eqs. (13), (17), and (18)) in a manner similar to that of Tai (ref. 6) and Kuhn and Nielsen (refs. 4 and 5). Equation (13) is solved for the normal velocity

$$\bar{v} = \frac{r}{r + n}\left(\bar{v}_w - \int_0^n \frac{\partial \bar{u}}{\partial s}\, d\eta\right) \tag{20}$$

and the n-momentum equation (eq. (18)) is integrated with respect to n to remove the n dependency and differentiated with respect to s to obtain the pressure gradient $\frac{\partial \bar{p}}{\partial s}$ as

$$\frac{\partial \bar{p}}{\partial s} = \frac{\partial \bar{p}_w}{\partial s} + 2\int_0^n \frac{\bar{u}}{r + n}\frac{\partial \bar{u}}{\partial s}\, d\eta - \int_0^n \frac{\bar{u}^2}{(r + n)^2}\frac{\partial r}{\partial s}\, d\eta \tag{21}$$

where η is a dummy variable of integration. Equations (20) and (21) are substituted into equation (17) and the resulting equation is multiplied by a weighting function

$$f(n) = n^{\sigma}; \quad \sigma = 0, 1 \tag{22}$$

and integrated completely across the boundary layer to yield the desired integral equation as

ORIGINAL PAGE IS
OF POOR QUALITY

ORIGINAL PAGE IS
OF POOR QUALITY

$$\int_0^{\delta} \left\{ \bar{u} \frac{\partial \bar{u}}{\partial s} + 2 \int_0^{n} \frac{\bar{u}}{r+\eta} \frac{\partial \bar{u}}{\partial s} \, d\eta - \left(\frac{\partial \bar{u}}{\partial n} + \frac{\bar{u}}{r+n} \right) \int_0^{n} \frac{\partial \bar{u}}{\partial s} \, d\eta \right.$$

$$+ \frac{\partial \bar{p}_w}{\partial s} - \frac{r+n}{r} \frac{1}{R_\infty} \left[\frac{\partial}{\partial n} \left(\beta_1 \frac{\partial \bar{u}}{\partial n} \right) + \frac{\beta_2}{r+n} \frac{\partial \bar{u}}{\partial n} - \frac{\beta_3 \bar{u}}{(r+n)^2} \right]$$

$$\left. - \int_0^{n} \frac{\bar{u}^2}{(r+\eta)^2} \frac{\partial r}{\partial s} \, d\eta + v_w \frac{\partial \bar{u}}{\partial n} + \frac{\bar{u}}{r+n} \right\} f(n) \, dn = 0 \qquad (23)$$

In equations (22) and (23), $\sigma = 0, 1$ corresponds to the momentum and moment-of-momentum equations, respectively.

The two equations derived from equation (23) using $\sigma = 0$ and 1 are sufficient to obtain solutions for the case of the weak interaction. For the case of the strong interaction, which might be expected to apply in the neighborhood of the fillet between the flat plate and ramp, an additional equation is required to obtain a solution. This equation is derived by integrating the continuity equation (13) completely across the boundary layer (essentially extending the limit n in equation (20) to δ) to get

$$\int_0^{\delta} \frac{\partial \bar{u}}{\partial s} \, d\eta = - \frac{r+\delta}{r} \bar{v}_e + \bar{v}_w \qquad (24)$$

Velocity Profile

The integration of equations (23) and (24) is accomplished by assuming a velocity profile that has the potential for indicating separated (reversed flow) characteristics in strong adverse pressure gradients. A profile that had satisfactory characteristics in subsonic and transonic flow on a convex surface was developed by Kuhn and Nielsen (ref. 4) and is utilized in this analysis

$$\bar{u} = \bar{u}_\tau \left[2.5 \ln (1 + n^+) + 5.1 - (3.387\, n^+ + 5.1)e^{-0.37n^+}\right] + 0.5\, \bar{u}_\beta \left[1 - \cos\left(\pi \frac{n}{\delta}\right)\right] \tag{25}$$

where $\bar{u}_\beta$ is the wake velocity and $\bar{u}_\tau$ is the friction velocity

$$\bar{u}_\tau = \left(\bar{\tau}_w / |\bar{\tau}_w|\right)\left(|\bar{\tau}_w| / \bar{\rho}_w\right)^{1/2} \tag{26}$$

In equation (25), the first term on the right-hand side represents the inner part of the velocity profile, consisting of a laminar sublayer whose function is to allow the no slip boundary conditions to be met at the wall and of the law-of-the-wall function. The second term represents the wake portion or outer part of the boundary layer by a cosine function that is easier to handle in the calculations than the more accurate error function representation.

Eddy Viscosity

The eddy viscosity model used in the present analysis is identical to that of Tai (ref. 6) which is similar to that of Kuhn and Nielsen (ref. 5).

The expressions for the eddy viscosity are given as follows:
For attached flow, inner layer

$$\beta = 1 + 0.0533 \left\{ e^{0.41 \frac{\bar{u}}{\bar{u}_\tau}} - \left[1 + 0.41 \frac{\bar{u}}{\bar{u}_\tau} + 0.5 \left(0.41 \frac{\bar{u}}{\bar{u}_\tau}\right)^2\right]\right\} \tag{27}$$

For attached flow, outer layer

ORIGINAL PAGE IS
OF POOR QUALITY

ORIGINAL PAGE IS
OF POOR QUALITY

$$\beta = \frac{0.013 + 0.0038\, e^{-\left[\frac{\delta^*}{\tau_w}\,\frac{dp}{ds}\,\frac{1}{15}\right]}}{\left[1 + 5.5\left(\frac{n}{\delta}\right)^6\right]}\,\bar{u}_e\,\delta^* R_\infty \tag{28}$$

For separated flow, inner layer

$$\beta = 1 + 0.018\,\bar{u}_e\, n\, R_{e_\infty}\left[1 - \left(\frac{\bar{u}}{\bar{u}_e}\right)^2\right] \tag{29}$$

For separated flow, outer layer

$$\beta = \frac{0.013\,\bar{u}_e\,\delta^*\,R_\infty}{\left[1 + 5.5\left(\frac{n}{\delta}\right)\right]^6} \tag{30}$$

System of Equations for Strong Interaction

Equation (25) is substituted into equations (23) and (24) with $\bar{u}_\beta$ being eliminated by evaluating $\bar{u}$ at $n = \delta$. Details as to how this is actually accomplished are given in Appendix B. Three ordinary differential equations are finally obtained with unknowns $\frac{d\bar{u}_\tau}{ds}$, $\frac{d\delta}{ds}$, and $\frac{d\bar{p}_w}{ds}$ which can be written in the matrix form

$$\begin{bmatrix} E_{11} & E_{12} & E_{13} \\ E_{21} & E_{22} & E_{23} \\ E_{31} & E_{32} & E_{33} \end{bmatrix} \begin{bmatrix} \frac{d\bar{u}_\tau}{ds} \\ \frac{d\delta}{ds} \\ \frac{d\bar{p}_w}{ds} \end{bmatrix} = \begin{bmatrix} Q_1 \\ Q_2 \\ Q_3 \end{bmatrix} \tag{31}$$

where the functions E_{ij} and Q_j are presented in Appendix C. Note that because of the existence of surface curvature effects the substitution of equation (21) into equation (17) makes it more convenient to make the wall pressure gradient $\frac{\partial \bar{p}_w}{\partial s}$ the third unknown in the present investigation rather than the velocity gradient at the edge of the boundary layer $\frac{\partial \bar{u}_e}{\partial s}$ as was done by Tai who had no such terms. Furthermore, the experimental pressure gradients with which theory is compared are wall pressure gradients.

Systems of Equations for Weak Interactions

Most of the calculations for the weak interaction case were made by an approach similar to that of Tai

$$\begin{bmatrix} E_{11} & E_{12} \\ E_{21} & E_{22} \end{bmatrix} \begin{bmatrix} \frac{d\bar{u}_\tau}{ds} \\ \frac{d\delta}{ds} \end{bmatrix} = \begin{bmatrix} Q_1 - E_{13} \frac{d\bar{p}_w}{ds} \\ Q_2 - E_{23} \frac{d\bar{p}_w}{ds} \end{bmatrix} \tag{32}$$

where E_{ij} and Q_j are identical to those in equation (31). As $\bar{u}_\tau$ tended toward zero near separation the coefficient determinant also tended toward zero with the result that the calculations diverged. For some of these conditions the solution algorithm was changed to

ORIGINAL PAGE IS
OE POOR QUALITY

ORIGINAL PAGE IS
OF POOR QUALITY

$$\begin{bmatrix} E_{12} & E_{13} \\ E_{22} & E_{23} \end{bmatrix} \begin{bmatrix} \frac{d\delta}{ds} \\ \frac{d\bar{p}_w}{ds} \end{bmatrix} = \begin{bmatrix} Q_1 - E_{11} \frac{d\bar{u}_\tau}{ds} \\ Q_2 - E_{21} \frac{d\bar{u}_\tau}{ds} \end{bmatrix} \tag{33}$$

where an initial value of $\bar{u}_\tau$ was prescribed by a parabolic arc extrapolation from previous stations so that the derivative $\frac{d\bar{u}_\tau}{ds}$ could be an input. The solutions of equation (33) were then iterated with the Prandtl-Meyer inviscid flow, with continuous updating of $\bar{u}_\tau$, until the velocities calculated for the outer edge of the boundary layer by the viscous equations (eq. (33)) matched the velocities computed for the Prandtl-Meyer flow.

Initial Conditions

Initial values for the boundary-layer variables were derived from Schlichting's equations for an incompressible flat plate boundary layer (ref. 11, pp. 433 and 468) modified for taking account of a pressure gradient

$$\bar{u}_\tau = \frac{0.171}{R_\infty^{0.1}} \frac{\bar{u}_e \left(1 + \frac{1.2}{m}\right)}{\left[\int_0^s \bar{u}_e \left(3.4 + \frac{2.4}{m}\right) ds\right]^{0.1}} \tag{34}$$

and

$$\delta^* = \frac{1.4}{\bar{u}_e^{3.4}} \left[\frac{K(m+1)}{mR_\infty^{\frac{1}{m}}} \int_0^s \bar{u}_e \left(3.4 + \frac{2.4}{m}\right) ds\right]^{\frac{m}{m+1}} \tag{35}$$

where

$$m = 4,\ k = 0.0128$$

These equations were derived assuming a 1/7th power velocity profile, hence, are not compatible with the velocity profile used in this investigation (eq. 25). Consequently, $\bar{u}_\tau$ and δ^* from equations (34) and (35) were iterated with the velocity profile of equation (25) to obtain new values of boundary-layer variables that were compatible both with that velocity profile and the pressure gradient existing at any particular iteration.

COUPLING OF INVISCID AND VISCOUS FLOWS

In the case of the strong interaction the requirements for the coupling of the inviscid and viscous flows are that both the magnitudes and directions of the velocities of the two flows match one another at the outer edge of the boundary layer. Because of entrainment of air from the inviscid into the viscous flow as the boundary layer grows along the surface, the slopes of the streamlines at the edge of the boundary layer are smaller than the slopes of the surface of the boundary layer $\frac{d\delta}{ds}$. The relation between the slopes is readily found by the use of the continuity equation to be

$$\frac{d\delta}{ds} = \tan \epsilon + \frac{1}{\bar{\rho}_e \bar{u}_e} \frac{d}{ds} [\bar{\rho}_e \bar{u}_e (\delta - \delta^*)] \tag{36}$$

which can be written as

$$\frac{d\delta^*}{ds} = \tan \epsilon + (\delta - \delta^*) \frac{d}{ds} \ln (\bar{\rho}_e \bar{u}_e) \tag{37}$$

ORIGINAL PAGE IS
OF POOR QUALITY

ORIGINAL PAGE IS
OF POOR QUALITY

and solved for the streamline angle

$$\epsilon = \tan^{-1} \left[\frac{d\delta^*}{ds} - (\delta - \delta^*) \frac{d}{ds} \ell n \, (\bar{\rho}_e \bar{u}_e)\right] \tag{38}$$

The normal velocity in the inviscid flow at the edge of the boundary layer is found from

$$v_{e,inv} = v_{inv} \sin \Theta \tag{39}$$

and the edge velocity $\bar{u}_e$ in the equation defining the assumed velocity distribution within the boundary layer, equation (25), is thus related to the inviscid flow by

$$\bar{u}_e = (v_{inv}^2 - v_{e,inv}^2)^{1/2} \tag{40}$$

For the case of the weak interaction the slopes of the inviscid streamlines are matched to the growth in boundary-layer displacement thickness $\frac{d\delta^*}{ds}$ and equation (38) reduces to

$$\epsilon = \tan^{-1} \left(\frac{d\delta^*}{ds}\right) \tag{41}$$

Also, the assumption is usually made that $v_{e,inv}$ is negligible, hence

$$\bar{u}_e = v_{inv} \tag{42}$$

Because of divergence problems that were encountered in the strong interaction calculations some weak interaction solutions were obtained both with and without this latter assumption.

COMPUTATIONAL METHODS

The numerical integrations of the viscous-flow equations in the s direction were carried out by means of a standard fourth-order Runge-Kutta method for both the point-iteration and global-iteration techniques. In the point-iteration technique the interaction between the viscous and inviscid flows was iterated at a constant s station until the solution converged, broke down or a prescribed number of iterations were completed. In the global-iteration method the boundary-layer calculations were executed over the complete s domain before reevaluation of the new inviscid pressure gradients and recalculation of the boundary layer. The computations were usually begun at $s = 0.20$ and continued downstream until the calculations broke down or an s of 1.5 was reached. Relaxation factors of varying magnitude were used on one or more of the dependent variables and various types of smoothing procedures were incorporated into the global-iteration calculations. All calculations presented herein were made with $\bar{v}_w$ equal to zero. For most calculations the Stewartson s transformation was ommitted because its effects were found to be generally negligible and its presence increased the complexity of the calculations.

As the calculations proceeded toward a separation point in the weak-interaction point-iteration method the solutions obtained by Tai's method, where $\frac{d\bar{u}_\tau}{ds}$ and $\frac{d\delta}{ds}$ were the unknown dependent variables, began to diverge because the determinant for the equations tended toward zero. For some cases

ORIGINAL PAGE IS
OF POOR QUALITY

the equations were revised so that $\frac{d\bar{u}_\tau}{ds}_{d\bar{u}_\tau}$ was prescribed and $\frac{d\delta}{ds}$ and $\frac{d\bar{p}_w}{ds}$ became the unknowns. The gradient $\frac{d\bar{u}_\tau}{ds}$ was initially prescribed by extrapolating $\bar{u}_\tau$ parabolically from the previous stations and calculating a three-point backward derivative using the extrapolated $\bar{u}_\tau$ as the third point. During the iterations $\bar{u}_\tau$ was continuously modified to require that the boundary-layer edge velocities in the inviscid and viscous flow were identical within prescribed limits. In many ways this type of calculation scheme seemed to be more naturally suited to supersonic flow problems than the approach used by Tai (ref. 6).

RESULTS AND DISCUSSION

General Comments on Stability and Convergence of Calculations

Before any final results of the calculations are presented it appears desirable to point out a few interesting or unusual characteristics that were encountered in making the computations that are not apparent from the final plots themselves. These are: the extreme instability of the calculations; the unusual values of relaxation factors that were required to allow the calculations to proceed; the ineffectiveness of the relaxation coefficients in improving convergence; and, finally, the inability to obtain any useful results using the strong-interaction or global-interaction techniques. (See ref. 14 for similar problems in instability in calculations in large adverse pressure gradients using a similar integral approach.)

First, there never was any problem in calculating the boundary-layer characteristics on the first iteration where the pressure gradient was assumed to be zero. As the boundary layer was iterated with the inviscid flow in the second and higher iterations many of the terms involved in the calculations tended to oscillate in value with the magnitude of the oscillations usually being catastrophically large. As an example, δ^* would often increase so much between adjacent stations as to make the

slope $\frac{d\delta^*}{ds}$ so large that the inviscid-flow calculations would indicate the existence of a detached shock with a subsonic inviscid flow above the boundary layer. This would abort the calculations because no provision had been made for the existence of subsonic flow this early in the investigation. Again, calculations would often abort because δ would become negative during the oscillations and no provision had been made in the equations for the interpretation of negative values of boundary-layer total thickness. In general, only a few of these types of problems could be solved without recourse to the introduction of relaxation factors.

The role of the relaxation factors was to introduce the interaction effects into the computations slowly and hence decrease the magnitude of the oscillations. Because of the magnitudes of the oscillations that existed without relaxation, numerical values of relaxation factors an order of magnitude smaller than usual had to be used. For example, in steep adverse pressure gradient regions but still some distance away from separation points, relaxation factors of 0.05 to 0.2 were required in the weak-interaction point-iteration method on two or more of the most critical terms to preserve order in the calculations. These small values of relaxation factor required about 200 iterations to permit satisfactory convergence. In the global-iteration scheme single relaxation factors on the order of 0.2 to 0.5 were sufficient, but this was because smoothing procedures were simultaneously employed.

A short study was made to determine the effects of relaxation factors on convergence. In the study no evidence was ever found that the use of relaxation factors converted a divergent solution into a convergent one. In fact, all evidence indicated that the use of relaxation factors in divergent solutions merely delayed the time required to reach the point where the computations broke down (i.e., larger number of iterations).

Attempts to obtain converged solutions by the strong-interaction technique were universally unsuccessful. In the point-iteration method these attempts included starting the calculations at $s = 0.20$ by the use of the usual initial procedures, starting the calculations just ahead of the fillet from the boundary layer determined by the weak-interaction

technique, and using a range of relaxation factors. Even the use of the global-interaction method resulted in divergent solutions for the flat plate.

In weak interactions converged solutions could be obtained by the use of the global-iteration technique combined with a cubic-spline smoothing procedure. Without smoothing, oscillations quickly began to appear in areas such as the junctures of the fillet with the approach surface and the ramp as the calculations proceeded downstream. The magnitude of these oscillations increased rapidly with increases in the number of iterations but without changes in location. Unfortunately, the smoothing procedure first controlled then decreased the magnitude of the oscillations by merely flattening the waves in both the upstream and downstream directions. Inasmuch as the positive and negative oscillations were completely out of phase with one another the oscillations were not properly cancelled and the converged solutions were obviously physically incorrect. In essence, the smoothing procedure allowed the errors from the critical points to seep in until the flow changes at the critical points were overwhelmed by the smoothing corrections, whence convergence could be achieved.

An examination was also made of the effects of grid size on stability of calculations and convergence. The results indicated no effect except to pinpoint more sharply the station at which divergence actually began.

Finally, the u_τ initially prescribed method appears to alleviate many of the previously mentioned problems, but its potential was not fully explored.

Effects of Various Terms or Parameters

Some final results computed by the weak-interaction method with point-iteration technique are presented in figure 2. In the figure, the non-dimensional wall-pressure ratio $\bar{p}_w$ and the local skin-friction coefficient c_f are plotted as functions of surface distance s for a range of wedge angles from 0° to 30°. The fillet is based on a 9th power polynomial and begins at $s = 0.98$ and ends at $s = 1.02$. Theoretical computations are represented by the lines; the symbols have been included at intervals only

to aid in identifying the curves. Only converged data are plotted. Data for $c_f > 0.0008$ were computed by the Tai method and data for $c_f < 0.0008$ for $\alpha = 30°$ were computed by the $\bar{u}_\tau$ initially-prescribed method. Similar calculations for $c_f < 0.0008$ were not made for the other wedge angles for reasons that will be discussed in the next section. The ticks on the pressure plot indicate the inviscid-flow pressure rises expected for the various wedge angles using shock equations.

The curves of figure 2 indicate that as the wedge angle increases the adverse pressure gradient also increases and the local skin-friction coefficient decreases. Boundary-layer separation was calculated for $\alpha = 30°$ at $s = 1.007$ and appears to be a probability for $\alpha = 25°$, $20°$, and $15°$. Note that the pressure rises lag changes in surface curvature. Approximately one-half of theoretical pressure rise at $\alpha = 10°$ occurs on the flat wedge surface downstream of the fillet. A comparison of the $\alpha = 10°$ calculations where no separation is indicated with some experimental data obtained at a Mach number of 2.75 (ref. 15) indicates (fig. 3) that, although the theoretical pressure rise occurs somewhat belatedly, it is in reasonable agreement with the experimental results.

Some nondimensional velocity profiles corresponding to the wedge angle of 30° are shown in figure 4. They corrobrate the appearance of separation. Note that practically all the significant boundary-layer profile changes occur in an extremely short region that corresponds to the steepest part of the adverse pressure gradient in figure 2.

At this point the question arises as to the possible effects the fillet could have on separation. Figure 5 shows that even for the larger wedge angles the effects of changing the size and, hence, radii of curvature of the fillet had very little effect on either the pressure or skin-friction distributions. Figure 6 shows that the surface curvature terms contributed little or nothing despite the relative smallness of the radii of curvature (lowest r/δ was about 2.9).

Finally, figure 7 indicates that sizable variations in the eddy-viscosity model were of no significance.

Calculations With Experimental Input

Although the results discussed in the previous section would appear to indicate the possibility of deriving a reasonable criterion for boundary-layer separation a closer examination reveals a serious problem. The data of figure 2, for example, indicate that separation occurs at wall pressure ratios approaching 3 or more whereas experiments such as those in references 12 and 16 and theoretical calculations such as those in reference 17 indicate that separation at $M_\infty = 3$ occurs for pressure ratios less than 2. In order to test this discrepancy some calculations were made using Law's (ref. 12) experimental pressure distribution for $\alpha = 25°$, where separation was well developed, to represent the final converged pressure distribution. The results are presented as figure 8. Included in figure 8 are the theoretical skin-friction results of Shang and Hankey (ref. 17) whose pressure distributions calculated by time-dependent Navier-Stokes methods are in reasonable agreement with Law's experimental data.

The data of figure 8 and the discussion in reference 12 indicate that boundary-layer separation occurred experimentally at an s of approximately 0.96 and a $\bar{p}_w$ of approximately 1.9. The calculations of Shang and Hankey (ref. 17) indicate separation at s approximately 0.95 and $\bar{p}_w$ about 1.03. Present calculations indicate separation at $s = 1.07$ and $\bar{p}_w = 4.3$. Furthermore, the experimental separation point occurs in the first pressure rise leading to the pressure plateau region whereas in the present investigation separation occurs in the second pressure rise at a much higher pressure in a region where a reattachment shock might be expected. This discrepancy is ascribed to the failure to provide in the present investigation for terms which can induce normal pressure gradients withou the need of surface curvature. This omission becomes even more serious for the cases where the ramp angle is large enough to force separation to occur well ahead of the fillet where there is no surface curvature and hence no mechanism for boundary-layer separation in the present approach. As illustrated in figure 9, due to the strong coelescence of the compression waves into a shock as one proceeds away from the surface, the pressure gradients at the wall

are considerably smaller than those at the outer edge of the boundary layer or the mean gradient that is essentially utilized in the integral-equation calculations. Omission of the terms that generate the normal pressure gradients also means ommission of the coelescence effects at the edge of the boundary layer and consequently much smaller mean axial pressure gradients than those that actually should exist. A similar serious problem was encountered by Werle and Bertke (ref. 18) in an investigation of the supersonic wedge problem wherein the boundary-layer equations were solved by a finite-difference approach. This concept was further substantiated in the present investigation by making some calculations wherein the pressure gradient within the first pressure rise was arbitrarily steepened without modification of the plateau pressure. Boundary-layer separation was readily achieved at the desired location. Additional evidence that normal pressure gradients in the boundary layer must be accounted for in integral methods is presented in reference 19 where the boundary layer is subsonic but is thick and has significant streamline curvature.

Modifications can be made to the integral-equation method to provide for a more realistic shock-boundary-layer interaction but at the present time the modifications will have to be either empirical or built up by interative inclusion of one or two more terms. From the standpoint of the desired end result the normal pressure gradients should not be prescribed a priori but should be an integral part of the interaction solution. In this respect, both the inviscid and viscous flow solutions in the present investigation are essentially one-dimensional calculations. It is possible that a practical solution of the shock-boundary-layer problem will require calculations in two dimensions. In view of the major deficiency just discussed in the present approach it was felt that further calculations without major modifications were not justified.

The strong normal pressure-gradient effects in shock-boundary-layer interactions are apparently peculiar to turbulent boundary layers. In laminar flows the pressure rises and pressure gradients, even at separation points, are an order of magnitude smaller and pose no major problems in the use of integral methods (ref. 20).

SUMMARY OF RESULTS

An investigation was made to determine the feasibility of using a boundary-layer integral method to study the separation of a turbulent boundary layer on a two-dimensional ramp at supersonic speeds. The numerical calculations were made for a free-stream Mach number of 3, a Reynolds number of 10 million, and over a ramp angle range from 0° to 30°.

For ramp angles where no flow separation was indicated, the theoretical calculations were in reasonable agreement with experimental data except for a somewhat belated rise in the pressure. For the larger ramp angles, where separation was present, the investigation produced results that were not in agreement with experiment or with results calculated by time-dependent Navier-Stokes methods apparently because no provision had been made for a proper shock-boundary layer interaction where strong normal pressure gradients are induced within the boundary layer under the shock independent of surface curvature. Within the limits of the calculations the effects of changes in the size of the fillet, the omission of curvature terms, and changes in eddy-viscosity model were negligible.

APPENDIX A

To avoid a singularity in the computations at the sharp corner C a fillet is introduced as indicated in figure 10. For best results it is desirable that the entry to the fillet at A and exit from the fillet at B be as smooth as possible and the smallest radii of curvature be concentrated close to the corner C. These conditions can most easily be attained by the use of a high-power polynomial wherein several of the higher order derivatives at A and B are set to zero. Preliminary calculations indicated that a 9th power polynomial would be optimum for the calculations. Some calculations were also made with a fillet based on a 7th power polynomial and an exponential shape which closely resembled the above shapes. Inasmuch as no data are shown for the last two shapes the details of the fillet are restricted to the 9th power polynomial case.

The shape of the fillet tangent to the flat plate at A and to the ramp at B where A and B are equidistant from C by the distance D is given by the 9th power polynomial

$$y = \sum_{i=0}^{9} C_i x^i \tag{A-1}$$

The boundary conditions are:

At point A

$$\left.\begin{aligned} y &= 0 \\ \frac{dy}{dx} = \frac{d^2y}{dx^2} = \frac{d^3y}{dx^3} = \frac{d^4y}{dx^4} &= 0 \end{aligned}\right\} \tag{A-2}$$

At point B

$$y = D \sin \alpha$$

$$\frac{dy}{dx} = \tan \alpha \qquad \text{(A-3)}$$

$$\frac{d^2y}{dx^2} = \frac{d^3y}{dx^3} = \frac{d^4y}{dx^4} = 0$$

ORIGINAL PAGE IS
OF POOR QUALITY

With the aid of the MIT algebraic computer language MACSYMA (ref. 21) the coefficients were found to be:

$$c_o = \frac{70D \cos^4\alpha \sin \alpha}{(1 + \cos\alpha)^9}$$

$$c_1 = \frac{\sin\alpha(350 \cos^5\alpha - 224 \cos^4\alpha + 84 \cos^3\alpha + 36 \cos^2\alpha + 9 \cos\alpha)}{\cos\alpha\ (1 + \cos\alpha)^9}$$

$$c_2 = \frac{140(5 \cos^2\alpha - 8 \cos\alpha + 5) \sin\alpha \cos\alpha}{D\ (1 + \cos\alpha)^9}$$

$$c_3 = \frac{140(\cos\alpha - 1)(5 \cos^2\alpha - 11 \cos\alpha + 5) \cos\alpha \sin\alpha}{D^2\ (1 + \cos\alpha)^9}$$

$$c_4 = \frac{70 \sin\alpha\ (5 \cos^4\alpha - 32 \cos^3\alpha + 52 \cos^2\alpha - 32 \cos\alpha + 5)}{D^3\ (1 + \cos\alpha)^9}$$

$$c_5 = \frac{70 \sin\alpha\ (\cos\alpha - 1)(\cos^4\alpha - 15 \cos^3\alpha + 31 \cos^2\alpha - 15 \cos\alpha + 1)}{D^4 \cos\alpha\ (1 + \cos\alpha)^9} \qquad \text{(A-4)}$$

$$c_6 = \frac{-28 \sin\alpha(8 \cos^4\alpha - 53 \cos^3\alpha + 88 \cos^2\alpha - 53 \cos\alpha + 8)}{D^5 \cos\alpha\ (1 + \cos\alpha)^9}$$

$$c_7 = \frac{140 \sin\alpha\ (\cos\alpha - 2)(\cos\alpha - 1)(2\cos\alpha - 1)}{D^6 \cos\alpha\ (1 + \cos\alpha)^9}$$

$$c_8 = \frac{-10 \sin\alpha\ (16 \cos^2\alpha - 31 \cos\alpha + 16)}{D^7 \cos\alpha\ (1 + \cos\alpha)^9}$$

$$c_9 = \frac{35 \sin\alpha\ (\cos\alpha - 1)}{D^8 \cos\alpha\ (1 + \cos\alpha)^9}$$

where α is the ramp angle and D is the distance from the corner to fillet tangency points. The radius of curvature r is computed as

$$r = \frac{\left[1 + \left(\frac{dy}{dx}\right)^2\right]^{3/2}}{\frac{d^2y}{dx^2}} \qquad \text{(A-5)}$$

The profile of the fillet for $D = .02$ and $\alpha = 30°$ is shown as a solid line in figure 10.

APPENDIX B

Incorporation of Velocity Profile into Integral Equation

The boundary-layer integral equation was derived in the main body of the paper as

$$\int_0^{\delta} \left\{ \bar{u} \frac{\partial \bar{u}}{\partial s} + 2 \int_0^n \frac{\bar{u}}{r+\eta} \frac{\partial \bar{u}}{\partial s} \, d\eta - \left(\frac{\partial \bar{u}}{\partial n} + \frac{\bar{u}}{r+n} \right) \int_0^n \frac{\partial \bar{u}}{\partial s} \, d\eta + \frac{\partial \bar{p}_w}{\partial s} \right.$$

$$- \frac{r+n}{r} \frac{1}{R_\infty} \left[\frac{\partial}{\partial n} \left(\beta_1 \frac{\partial \bar{u}}{\partial n} \right) + \frac{\beta_2}{r+n} \frac{\partial \bar{u}}{\partial n} - \frac{\beta_3 \bar{u}}{(r+n)^2} \right]$$

$$\left. - \int_0^n \frac{\bar{u}^2}{(r+\eta)^2} \frac{dr}{ds} \, d\eta + v_w \left(\frac{\partial \bar{u}}{\partial n} + \frac{\bar{u}}{r+n} \right) \right\} f(n) \, dn = 0 \qquad (23)$$

The assumed velocity profile that must be incorporated into the above integral equation is

$$\bar{u} = \bar{u}_\tau \left[2.5 \, \ell n \, (1 + n^+) + 5.1 - (3.387 \, n^+ + 5.1) e^{-0.37 n^+} \right]$$

$$+ 0.5 \, \bar{u}_\beta \left[1 - \cos \left(\pi \frac{n}{\delta} \right) \right] \qquad (25)$$

In order to develop an expression for $\frac{\partial \bar{u}}{\partial s}$ note that $\bar{u}$ is a function of several variables that are in turn functions of s, hence, let

$$\bar{u} = [\bar{u}_\beta(s), \bar{u}_\tau(s), \delta(s)] \tag{B-1}$$

or

$$\frac{\partial \bar{u}}{\partial s} = \frac{\partial \bar{u}}{\partial \bar{u}_\beta} \frac{\partial \bar{u}_\beta}{\partial s} + \frac{\partial \bar{u}}{\partial \bar{u}_\tau} \frac{\partial \bar{u}_\tau}{\partial s} + \frac{\partial \bar{u}}{\partial \delta} \frac{\partial \delta}{\partial s} \tag{B-2}$$

Also, let

$$\bar{u}_e = \bar{u}_e [\bar{u}_\beta(s), \bar{u}_\tau(s), \delta(s)] \tag{B-3}$$

or

$$\frac{\partial \bar{u}_e}{\partial s} = \frac{\partial \bar{u}_e}{\partial \bar{u}_\beta} \frac{\partial \bar{u}_\beta}{\partial s} + \frac{\partial \bar{u}_e}{\partial \bar{u}_\tau} \frac{\partial \bar{u}_\tau}{\partial s} + \frac{\partial \bar{u}_e}{\partial \delta} \frac{\partial \delta}{\partial s} \tag{B-4}$$

Boundary conditions at $n = \delta$

$$\bar{u} = \bar{u}_e$$

and

$$\frac{\partial \bar{u}_e}{\partial \bar{u}_\beta} = 1 \tag{B-5}$$

Substitution of equation (B-5) into equation (B-4), followed by the elimination of $\frac{\partial \bar{u}_\beta}{\partial s}$ from equation (B-2) with the use of the resultant

equation (B-4) yields

$$\frac{\partial \bar{u}}{\partial s} = \left(\frac{\partial \bar{u}}{\partial \bar{u}_\tau} - \frac{\partial \bar{u}}{\partial \bar{u}_\beta}\frac{\partial \bar{u}_e}{\partial \bar{u}_\tau}\right)\frac{\partial \bar{u}_\tau}{\partial s} + \left(\frac{\partial \bar{u}}{\partial \delta} - \frac{\partial \bar{u}}{\partial \bar{u}_\beta}\frac{\partial \bar{u}_e}{\partial \delta}\right)\frac{\partial \delta}{\partial s} + \frac{\partial \bar{u}}{\partial \bar{u}_\beta}\frac{\partial \bar{u}_e}{\partial s} \quad \text{(B-6)}$$

The derivatives $\frac{\partial \bar{u}_e}{\partial \bar{u}_\tau}$ and $\frac{\partial \bar{u}_e}{\partial \delta}$ are not functions of n and it is convenient to remove them from the equation by differentiating equation (25) to give

$$\frac{\partial \bar{u}_e}{\partial \bar{u}_\tau} = a_1 = 2.5 \ln (1 + \delta^+) - (4.887 - 1.25319\delta^+)\,\delta^+ e^{-0.37\delta^+} + 5.1\,(1 - e^{-0.37\delta^+}) + \frac{2.5\delta^+}{1 + \delta^+} \quad \text{(B-7)}$$

where $\delta^+ = \frac{|\hat{u}_\tau|\hat{n}}{\hat{\nu}}$, and

$$\frac{\partial \bar{u}_e}{\partial \delta} = a_2 = \bar{u}_\tau |\bar{u}_\tau| R_\infty \left[\frac{2.5}{1 + \delta^+} - (1.5 - 1.25319\delta^+)e^{-0.37\delta^+}\right] \quad \text{(B-8)}$$

so that equation (B-6) can be written in the form

$$\frac{\partial \bar{u}}{\partial s} = \left(\frac{\partial \bar{u}}{\partial \bar{u}_\tau} - a_1 \frac{\partial \bar{u}}{\partial \bar{u}_\beta}\right)\frac{\partial \bar{u}_\tau}{\partial s} + \left(\frac{\partial \bar{u}}{\partial \delta} - a_2 \frac{\partial \bar{u}}{\partial \bar{u}_\beta}\right)\frac{\partial \delta}{\partial s} + \frac{\partial \bar{u}}{\partial \bar{u}_\beta}\frac{\partial \bar{u}_e}{\partial s} \quad \text{(B-9)}$$

The remaining derivatives in the coefficients for $\frac{\partial \bar{u}_\tau}{\partial s}$, $\frac{\partial \delta}{\partial s}$, and $\frac{\partial \bar{u}_e}{\partial s}$ in equation (B-9) are functions of n. Expressions for these derivatives can

readily be deduced from equation (25) but are not reproduced here.

In the region of the ramp fillet centrifugal forces will affect the boundary-layer edge velocity $\bar{u}_e$ if the radius of curvature exceeds the boundary-layer thickness δ. Consequently, the necessity that the edge velocities computed by the boundary-layer equations match those computed from Prandtl-Meyer invicid flow requires that the unknown derivative $\frac{\partial \bar{u}_e}{\partial s}$ be replaced by a new unknown $\frac{\partial \bar{p}_w}{\partial s}$. Put $n = \delta$ in equations (21), (17), and (20) to obtain, respectively

$$\frac{\partial \bar{p}_e}{\partial s} = \frac{\partial \bar{p}_w}{\partial s} + 2 \int_0^\delta \frac{\bar{u}}{r + n} \frac{\partial \bar{u}}{\partial s} \, dn - \int_0^\delta \frac{\bar{u}^2}{(r + n)^2} \frac{dr}{ds} \, dn \tag{B-10}$$

$$\frac{r}{r + \delta} \bar{u}_e \frac{\partial \bar{u}_e}{\partial s} + \frac{\bar{v}_e \bar{u}_e}{r + \delta} = - \frac{r}{r + \delta} \frac{\partial \bar{p}_e}{\partial s} + \frac{1}{R_\infty} \frac{\bar{u}_e}{(r + \delta)^2} \tag{B-11}$$

(where the assumption was made that viscous effects at the edge of the boundary layer are small)

$$\bar{v}_e = - \frac{r}{r + \delta} \left(\int_0^\delta \frac{\partial \bar{u}}{\partial s} \, dn - \bar{v}_w \right) \tag{B-12}$$

Elimination of $\frac{\partial \bar{p}_e}{\partial s}$ and $\bar{v}_e$ from equation (B-11) by use of equations (B-10) and (B-11) results in

$$\frac{\partial \bar{u}_e}{\partial s} = - \frac{1}{\bar{u}_e} \frac{\partial \bar{p}_w}{\partial s} - \frac{2}{\bar{u}_e} \int_0^\delta \frac{\bar{u}}{(r + n)} \frac{\partial \bar{u}}{\partial s} \, dn + \frac{1}{\bar{u}_e} \int_0^\delta \frac{\bar{u}^2}{(r + n)^2} \frac{dr}{ds} \, dn$$

ORIGINAL PAGE IS
OF POOR QUALITY

$$+ \frac{1}{r+\delta} \int_0^{\delta} \frac{\partial \bar{u}}{\partial s}\, dn + \frac{1}{R_\infty} \frac{1}{r(r+\delta)} - \frac{\bar{v}_w}{r+\delta} \qquad \text{(B-13)}$$

Substitution of the expression for $\frac{\partial \bar{u}}{\partial s}$ from equation (B-9) into equation (B-13) yields after some simplification

$$\frac{\partial \bar{u}_e}{\partial s} = -\frac{P_1}{\bar{u}_e} \frac{\partial \bar{p}_w}{\partial s} + \frac{P_1}{R_\infty} \frac{1}{r(r+\delta)} - \frac{P_1 \bar{v}_w}{(r+\delta)} + \frac{P_1}{\bar{u}_e} \int_0^{\delta} \frac{\bar{u}^2}{(r+n)^2} \frac{dr}{ds}\, dn$$

$$+ (-P_1 P_2 + P_1 P_4) \frac{\partial \bar{u}_\tau}{\partial s} + (-P_1 P_3 + P_1 P_5) \frac{\partial \delta}{\partial s} \qquad \text{(B-14)}$$

where

$$\left.\begin{aligned}
P_1 &= \left[1 + \frac{2\delta}{\bar{u}_e} \int_0^1 \frac{\bar{u}}{r+n} \frac{\partial \bar{u}}{\partial \bar{u}_\beta}\, d\left(\frac{n}{\delta}\right) - \frac{\delta}{r+\delta} \int_0^1 \frac{\partial \bar{u}}{\partial \bar{u}_\beta}\, d\left(\frac{n}{\delta}\right) \right]^{-1} \\
P_2 &= \frac{2\delta}{\bar{u}_e} \int_0^1 \frac{\bar{u}}{r+n} \left(\frac{\partial \bar{u}}{\partial \bar{u}_\tau} - a_1 \frac{\partial \bar{u}}{\partial \bar{u}_\beta} \right) d\left(\frac{n}{\delta}\right) \\
P_3 &= \frac{2\delta}{\bar{u}_e} \int_0^1 \frac{\bar{u}}{r+n} \left(\frac{\partial \bar{u}}{\partial \delta} - a_2 \frac{\partial \bar{u}}{\partial \bar{u}_\beta} \right) d\left(\frac{n}{\delta}\right) \\
P_4 &= \frac{\delta}{r+\delta} \int_0^1 \left(\frac{\partial \bar{u}}{\partial \bar{u}_\tau} - a_1 \frac{\partial \bar{u}}{\partial \bar{u}_\beta} \right) d\left(\frac{n}{\delta}\right) \\
P_5 &= \frac{\delta}{r+\delta} \int_0^1 \left(\frac{\partial \bar{u}}{\partial \delta} - a_2 \frac{\partial \bar{u}}{\partial \bar{u}_\beta} \right) d\left(\frac{n}{\delta}\right)
\end{aligned}\right\} \qquad \text{(B-15)}$$

Next, substitution of $\frac{\partial \bar{u}_e}{ds}$ from equation (B-14) into equation (B-9) produces

$$\frac{\partial \bar{u}}{\partial s} = \left[\frac{\partial \bar{u}}{\partial u_\tau} - \frac{\partial \bar{u}}{\partial \bar{u}_\beta}(P_1P_2 - P_1P_4 + a_1)\right] + \frac{P_1}{R_\infty r(r+\delta)}\frac{\partial \bar{u}}{\partial \bar{u}_\beta}$$

$$+\left[\frac{\partial \bar{u}}{\partial \delta} - \frac{\partial \bar{u}}{\partial \bar{u}_\beta}(P_1P_3 - P_1P_5 + a_2)\right] - \frac{P_1}{\bar{u}_e}\frac{\partial \bar{u}}{\partial \bar{u}_\beta}\frac{\partial p_w}{\partial s} \qquad \text{(B-16)}$$

$$- P_1\frac{\partial \bar{u}}{\partial \bar{u}_\beta}\frac{\bar{v}_w}{r+\delta} + \frac{P_1}{\bar{u}_e}\int_0^\delta \frac{\bar{u}^2}{(r+n)^2}\frac{dr}{ds}\,dn$$

Finally, the expression for $\frac{\partial \bar{u}}{\partial s}$ from equation (B-16) is substituted into equations (23) and (24) for the strong interaction case and equation (23) for the weak interaction case to yield, after collection of like unknown terms, the algebraic equations

$$\begin{bmatrix} E_{11} & E_{12} & E_{13} \\ E_{21} & E_{22} & E_{23} \\ E_{31} & E_{32} & E_{33} \end{bmatrix} \begin{bmatrix} \frac{d\bar{u}_\tau}{ds} \\ \frac{d\delta}{ds} \\ \frac{d\bar{p}_w}{ds} \end{bmatrix} = \begin{bmatrix} Q_1 \\ Q_2 \\ Q_3 \end{bmatrix} \qquad (31)$$

for the strong interaction and

$$\begin{bmatrix} E_{11} & E_{12} \\ E_{21} & E_{22} \end{bmatrix} \begin{bmatrix} \frac{d\bar{u}_\tau}{ds} \\ \frac{d\delta}{ds} \end{bmatrix} = \begin{bmatrix} Q_1 - E_{13}\frac{d\bar{p}_w}{ds} \\ Q_2 - E_{23}\frac{d\bar{p}_w}{ds} \end{bmatrix} \qquad (32)$$

ORIGINAL PAGE IS
OF POOR QUALITY

or

$$\begin{bmatrix} E_{12} & E_{13} \\ E_{22} & E_{23} \end{bmatrix} \begin{bmatrix} \frac{d\delta}{ds} \\ \frac{d\bar{p}_w}{ds} \end{bmatrix} = \begin{bmatrix} Q_1 - E_{11} \frac{du_\tau}{ds} \\ Q_2 - E_{21} \frac{du_\tau}{ds} \end{bmatrix} \tag{33}$$

for the weak interaction.

The coefficients or functions E_{ij} and Q_j are given in Appendix C.

APPENDIX C

The Functions E_{ij} and Q_j

The E_{ij}'s and Q_j's in equations (32) are as follows

$$E_{11} = \int_0^1 \left(2\frac{\bar{u}}{\bar{u}_e} - 1\right)\left[\frac{\partial \bar{u}}{\partial \bar{u}_\tau} - \frac{\partial \bar{u}}{\partial \bar{u}_\beta}(a_1 + P_1P_2 - P_1P_4)\right] d\left(\frac{n}{\delta}\right)$$

$$- \int_0^1 \frac{\delta}{r+n}\frac{\bar{u}}{\bar{u}_e}\int_0^{\frac{n}{\delta}}\left[\frac{\partial \bar{u}}{\partial \bar{u}_\tau} - \frac{\partial \bar{u}}{\partial \bar{u}_\beta}(a_1 + P_1P_2 - P_1P_4)\right] d\left(\frac{n}{\delta}\right) d\left(\frac{n}{\delta}\right)$$

$$+ 2\int_0^1 \int_0^{\frac{n}{\delta}} \frac{\delta}{r+n}\frac{\bar{u}}{\bar{u}_e}\left[\frac{\partial \bar{u}}{\partial \bar{u}_\tau} - \frac{\partial \bar{u}}{\partial \bar{u}_\beta}(a_1 + P_1P_2 - P_1P_4)\right] d\left(\frac{n}{\delta}\right) d\left(\frac{n}{\delta}\right) \qquad (C\text{-}1)$$

$$E_{12} = \int_0^1 \left(2\frac{\bar{u}}{\bar{u}_e} - 1\right)\left[\frac{\partial \bar{u}}{\partial \delta} - \frac{\partial \bar{u}}{\partial \bar{u}_\beta}(a_2 + P_1P_3 - P_1P_5)\right] d\left(\frac{n}{\delta}\right)$$

$$- \int_0^1 \frac{\delta}{r+n}\frac{\bar{u}}{\bar{u}_e}\int_0^{\frac{n}{\delta}}\left[\frac{\partial \bar{u}}{\partial \delta} - \frac{\partial \bar{u}}{\partial \bar{u}_\beta}(a_2 + P_1P_3 - P_1P_5)\right] d\left(\frac{n}{\delta}\right) d\left(\frac{n}{\delta}\right)$$

$$+ 2\int_0^1 \int_0^{\frac{n}{\delta}} \frac{\delta}{r+n}\frac{\bar{u}}{\bar{u}_e}\left[\frac{\partial \bar{u}}{\partial \delta} - \frac{\partial \bar{u}}{\partial \bar{u}_\beta}(a_2 + P_1P_3 - P_1P_5)\right] d\left(\frac{n}{\delta}\right) d\left(\frac{n}{\delta}\right)$$

$$+ \frac{\bar{u}_e}{\delta}\int_0^1 \left(\frac{\bar{u}}{\bar{u}_e}\right)^2 \frac{n}{r+n}\, d\left(\frac{n}{\delta}\right) \qquad (C\text{-}2)$$

$$E_{13} = -\frac{P_1}{\bar{u}_e}\int_0^1 \left(2\frac{\bar{u}}{\bar{u}_e} - 1\right)\frac{\partial \bar{u}}{\partial \bar{u}_\beta}\, d\left(\frac{n}{\delta}\right)$$

$$+ \frac{P_1}{\bar{u}_e}\int_0^1 \frac{\delta}{r+n}\,\frac{\bar{u}}{\bar{u}_e}\int_0^{\frac{n}{\delta}} \frac{\partial \bar{u}}{\partial \bar{u}_\beta}\, d\left(\frac{\eta}{\delta}\right) d\left(\frac{n}{\delta}\right)$$

$$- 2\frac{P_1}{\bar{u}_e}\int_0^1 \int_0^{\frac{n}{\delta}} \frac{\delta}{r+\eta}\,\frac{\bar{u}}{\bar{u}_e}\,\frac{\partial \bar{u}}{\partial \bar{u}_\beta}\, d\left(\frac{\eta}{\delta}\right) d\left(\frac{n}{\delta}\right) + \frac{1}{\bar{u}_e} \qquad \text{(C-3)}$$

$$E_{21} = \int_0^1 F(n)\left[\frac{\partial \bar{u}}{\partial \bar{u}_\tau} - \frac{\partial \bar{u}}{\partial \bar{u}_\beta}\,(a_1 + P_1P_2 - P_1P_4)\right] d\left(\frac{n}{\delta}\right)$$

$$+ \int_0^1 \frac{r\delta}{(r+n)^2}\left[\int_0^{\frac{n}{\delta}} \frac{\bar{u}}{\bar{u}_e}\, d\left(\frac{\eta}{\delta}\right)\right]\left\{\int_0^{\frac{n}{\delta}}\left[\frac{\partial \bar{u}}{\partial \bar{u}_\tau} - \frac{\partial \bar{u}}{\partial \bar{u}_\beta}\,(a_1 + P_1P_2 - P_1P_4)\right] d\left(\frac{\eta}{\delta}\right)\right\} d\left(\frac{n}{\delta}\right)$$

$$+ 2\int_0^1 \frac{n}{\delta}\int_0^{\frac{n}{\delta}} \frac{\delta}{r+\eta}\,\frac{\bar{u}}{\bar{u}_e}\left[\frac{\partial \bar{u}}{\partial \bar{u}_\tau} - \frac{\partial \bar{u}}{\partial \bar{u}_\beta}\,(a_1 + P_1P_2 - P_1P_4)\right] d\left(\frac{\eta}{\delta}\right) d\left(\frac{n}{\delta}\right) \qquad \text{(C-4)}$$

$$E_{22} = \int_0^1 F(n) \left[\frac{\partial \bar{u}}{\partial \delta} - \frac{\partial \bar{u}}{\partial \bar{u}_\beta} (a_2 + P_1 P_3 - P_1 P_5) \right] d\left(\frac{n}{\delta}\right)$$

$$+ \int_0^1 \frac{r\delta}{(r+n)^2} \int_0^{\frac{n}{\delta}} \left[\frac{\bar{u}}{\bar{u}_e} d\left(\frac{\eta}{\delta}\right) \right] \left\{ \int_0^{\frac{n}{\delta}} \left[\frac{\partial \bar{u}}{\partial \delta} - \frac{\partial \bar{u}}{\partial \bar{u}_\beta} (a_2 + P_1 P_3 - P_1 P_5) \right] d\left(\frac{\eta}{\delta}\right) \right\} d\left(\frac{n}{\delta}\right)$$

$$+ 2 \int_0^1 \frac{n}{\delta} \int_0^{\frac{n}{\delta}} \frac{\delta}{r+\eta} \frac{\bar{u}}{\bar{u}_e} \left[\frac{\partial \bar{u}}{\partial \bar{u}_\beta} (a_2 + P_1 P_3 - P_1 P_5) \right] d\left(\frac{\eta}{\delta}\right) d\left(\frac{n}{\delta}\right)$$

$$+ \frac{\bar{u}_e}{\delta} \int_0^1 \left(\frac{\bar{u}}{\bar{u}_e} \right)^2 \frac{n}{\delta} \frac{n}{r+n} d\left(\frac{n}{\delta}\right) \qquad \text{(C-5)}$$

$$E_{23} = - \frac{P_1}{\bar{u}_e} \int_0^1 F(n) \frac{\partial \bar{u}}{\partial \bar{u}_\beta} d\left(\frac{n}{\delta}\right)$$

$$- \frac{P_1}{\bar{u}_e} \int_0^1 \frac{r\delta}{(r+n)^2} \left[\int_0^{\frac{n}{\delta}} \frac{\bar{u}}{\bar{u}_e} d\left(\frac{\eta}{\delta}\right) \right] \left[\int_0^{\frac{n}{\delta}} \frac{\partial \bar{u}}{\partial \bar{u}_\beta} d\left(\frac{\eta}{\delta}\right) \right] d\left(\frac{n}{\delta}\right)$$

$$- \frac{2P_1}{\bar{u}_e} \int_0^1 \frac{n}{\delta} \int_0^{\frac{n}{\delta}} \frac{\delta}{r+\eta} \frac{\bar{u}}{\bar{u}_e} \frac{\partial \bar{u}}{\partial \bar{u}_\beta} d\left(\frac{\eta}{\delta}\right) d\left(\frac{n}{\delta}\right) + \frac{1}{2\bar{u}_e} \qquad \text{(C-6)}$$

$$E_{31} = \int_0^1 \left[\frac{\partial \bar{u}}{\partial \bar{u}_\tau} - \frac{\partial \bar{u}}{\partial \bar{u}_\beta} (a_1 + P_1 P_2 - P_1 P_4) \right] d(\frac{n}{\delta}) \tag{C-7}$$

$$E_{32} = \int_0^1 \left[\frac{\partial \bar{u}}{\partial \delta} - \frac{\partial \bar{u}}{\partial \bar{u}_\beta} (a_2 + P_1 P_3 - P_1 P_5) \right] d(\frac{n}{\delta}) \tag{C-8}$$

$$E_{33} = - \frac{P_1}{\bar{u}_e} \int_0^1 \frac{\partial \bar{u}}{\partial \bar{u}_\beta} d(\frac{n}{\delta}) \tag{C-9}$$

$$Q_1 = P_1 \left[\frac{1}{R_\infty \, r(r + \delta)} + \frac{\bar{u}_e}{\delta} \int_0^1 \left(\frac{\bar{u}}{\bar{u}_e} \frac{\delta}{r + n} \right)^2 \frac{dr}{ds} \, d(\frac{n}{\delta}) \right.$$

$$\left. - \frac{v_w}{r + \delta} \right] \left[- \int_0^1 (2 \frac{\bar{u}}{\bar{u}_e} - 1) \frac{\partial \bar{u}}{\partial \bar{u}_\beta} d(\frac{n}{\delta}) + \int_0^1 \frac{\delta}{r+n} \frac{\bar{u}}{\bar{u}_e} \int_0^{\frac{n}{\delta}} \frac{\partial \bar{u}}{\partial \bar{u}_\beta} d(\frac{\eta}{\delta}) \, d(\frac{n}{\delta}) \right.$$

$$- 2 \int_0^1 \int_0^{\frac{n}{\delta}} \frac{\delta}{r + \eta} \frac{\bar{u}}{\bar{u}_e} \frac{\partial \bar{u}}{\partial \bar{u}_\beta} d(\frac{\eta}{\delta}) \, d(\frac{n}{\delta}) + \frac{1}{R_\infty} \left\{ - \frac{\beta_1 (s_1 o)}{\delta \, \bar{u}_e} \frac{\partial \bar{u}}{\partial n} \Big|_w \right.$$

$$\left. + \frac{1}{r \bar{u}_e} \left[\int_0^1 (\beta_2 - \beta_1) \frac{\partial \bar{u}}{\partial n} d(\frac{n}{\delta}) - \int_0^1 \frac{\beta_3 \bar{u}}{r + n} d(\frac{n}{\delta}) \right] \right\}$$

$$\left. + \frac{\bar{u}_e}{\delta} \int_0^1 \int_0^{\frac{n}{\delta}} \frac{\bar{u}}{\bar{u}_e} \left(\frac{\delta}{r + \eta} \right)^2 \frac{dr}{ds} \, d(\frac{\eta}{\delta}) \, d(\frac{n}{\delta}) - v_w \left[\frac{1}{\delta} + \int_0^1 \frac{\bar{u}}{\bar{u}_e} \frac{1}{r + n} d(\frac{n}{\delta}) \right] \right.$$

(C-10)

$$Q_2 = P_1 \left[\frac{1}{R_\infty\, r(r+\delta)} + \frac{\bar{u}_e}{\delta} \int_0^1 \left(\frac{\bar{u}}{\bar{u}_e} \frac{\delta}{r+n} \right) \frac{dr}{ds}\; d\left(\frac{n}{\delta}\right) \right.$$

$$\left. - \frac{v_w}{r+\delta} \right] \left\{ - \int_0^1 F(n)\, \frac{\partial \bar{u}}{\partial \bar{u}_\beta}\, d\left(\frac{n}{\delta}\right) - \int_0^1 \frac{r\delta}{(r+n)^2} \left[\int_0^{\frac{n}{\delta}} \frac{\bar{u}}{\bar{u}_e}\; d\left(\frac{\eta}{\delta}\right) \right] \right. \times$$

$$\left. \left[\int_0^{\frac{n}{\delta}} \frac{\partial \bar{u}}{\partial \bar{u}_\beta}\; d\left(\frac{\eta}{\delta}\right) \right] d\left(\frac{n}{\delta}\right) - 2 \int_0^1 \frac{n}{\delta} \int_0^{\frac{n}{\delta}} \frac{\delta}{r+\eta}\, \frac{\bar{u}}{\bar{u}_e}\, \frac{\partial \bar{u}}{\partial \bar{u}_\beta}\, d\left(\frac{\eta}{\delta}\right)\, d\left(\frac{n}{\delta}\right) \right\}$$

$$+ \frac{1}{R_\infty\, \delta\, u_e} \left[- \int_0^1 \frac{r+2n}{r}\, \beta_1\, \frac{\partial \bar{u}}{\partial n}\; d\left(\frac{n}{\delta}\right) + \int_0^1 \frac{n}{r}\, \beta_2\, \frac{\partial \bar{u}}{\partial n}\; d\left(\frac{n}{\delta}\right) \right.$$

$$\left. - \int_0^1 \frac{n}{r(r+n)}\; \beta_3\, \bar{u}\, d\left(\frac{n}{\delta}\right) \right] + \frac{\bar{u}_e}{\delta} \int_0^1 \frac{n}{\delta} \int_0^{\frac{n}{\delta}} \left(\frac{\bar{u}}{\bar{u}_e} \frac{\delta}{r+\eta} \right)^2 \frac{dr}{ds}\; d\left(\frac{\eta}{\delta}\right)\, d\left(\frac{n}{\delta}\right)$$

$$- \frac{\bar{v}_w}{\bar{u}_e} \int_0^1 \frac{n}{\delta} \left(\frac{\partial \bar{u}}{\partial n} + \frac{\bar{u}}{r+n} \right) d\left(\frac{n}{\delta}\right) \qquad \text{(C-11)}$$

$$Q_3 = - P_1 \left[\frac{1}{R_\infty r(r+\delta)} + \frac{\bar{u}_e}{\delta} \int_0^1 \left(\frac{\bar{u}}{\bar{u}_e} \frac{\delta}{r+n} \right)^2 \frac{dr}{ds}\; d\left(\frac{n}{\delta}\right) - \frac{\bar{v}_w}{r+\delta} \right] \int_0^1 \frac{\partial \bar{u}}{\partial \bar{u}_\beta}\; d\left(\frac{n}{\delta}\right)$$

$$+ \frac{\bar{v}_w}{\delta} - \frac{r+\delta}{r}\; \frac{\bar{v}_e}{\delta} \qquad \text{(C-12)}$$

where

$$F(n) = 2\frac{\bar{u}}{\bar{u}_e}\frac{n}{\delta} - 1 + \frac{r}{r+\delta}\int_0^1 \frac{\bar{u}}{\bar{u}_e}\, d\left(\frac{n}{\delta}\right) - \frac{r}{r+n}\int_0^{n/\delta} \frac{\bar{u}}{\bar{u}_e}\, d\left(\frac{\eta}{\delta}\right) \qquad \text{(C-13)}$$

and where P_1, P_2, P_3, P_4, P_5 and a_1, a_2 have been defined in Appendix B. For $r >> \delta$ these functions reduce to those of Tai (ref. 6).

REFERENCES

1. Hung, C. M.; and MacCormack, R. W.: Numerical Simulation of Supersonic and Hypersonic Turbulent Compression Corner Flows Using Relaxation Models. AIAA Paper No. 76-410, July 1976.

2. Shang, J. S.; Hankey, W. L., Jr.; and Law, C. Herbert: Numerical Simulation of Shock Wave-Turbulent Boundary Layer Interaction. AIAA Paper No. 76-95, Jan. 1976.

3. Patel, D. K.; and Czarnecki, K. R.: Theoretical Face Pressure and Drag Characteristics of Forward-Facing Steps in Supersonic Turbulent Boundary Layers. NASA TN D-8040, 1975.

4. Kuhn, Gary D.; and Nielsen, Jack N.: An Analytical Method for Calculating Turbulent Separated Flows Due to Adverse Pressure Gradients. Project Squid Headquarters, Technical Report NEAR-1-PU, N72-16234, Oct. 1971.

5. Kuhn, Gary D.; and Nielsen, Jack N.: Prediction of Turbulent Separated Boundary Layers. AIAA Paper No. 73-663, July 1973.

6. Tai, Tsze C.: Transonic Turbulent Viscous-Inviscid Interaction Over Airfoils. AIAA Paper No. 75-78, Jan. 1975.

7. Stewartson, K.: Correlated Incompressible and Compressible Boundary Layers. Proc. Roy. Soc., Sec. A, vol. 200, 1949, pp. 85-100.

8. Ames Research Staff: Equations, Tables and Charts for Compressible Flow. NACA TR-1135, 1953.

9. Sommer, Simon C.; and Short, Barbara J.: Free-Flight Measurements of Turbulent-Boundary-Layer Skin Friction in the Presence of Severe Aerodynamic Heating at Mach Numbers from 2.8 to 7.0. NACA TN 3391, 1955.

10. Lin, C. C., *ed.*: *High-Speed Aerodynamics and Jet Propulsion.* Vol. V, Turbulent Flows and Heat Transfer. Princeton Univ. Press, Princeton, N.J., 1959, pp. 113-116.

11. Schlichting, Hermann: Boundary Layer Theory. Pergamon Press, New York, 1st Ed., 1955, p. 98, 433, 468.

12. Law, C. H.: Supersonic Turbulent Boundary Layer Separation. AIAA J., vol. 12, no. 6, June 1974, pp. 794-797.

13. Sandborn, V. A.: A Review of Turbulence Measurements in Compressible Flow. NASA TM X-62, 337, 1974.

14. Altstatt, M. C.: An Experimental and Analytic Investigation of a Transonic Shock-Wave/Boundary-Layer Investigation. AEDC-TR-77-47.

15. Drougge, George: Experimental Investigation of the Influence of String Adverse Pressure Gradients on Turbulent Boundary Layer at Supersonic Speeds. Eighth International Congress for Theoretical and Applied Mechanics, Istanbul, Turkey, 1952.

16. Czarnecki, K. R.; and Jackson, Mary W.: Turbulent Boundary-Layer Separation Due to a Forward-Facing Step. AIAA J., vol. 13, Dec. 1975, pp. 1585-1591.

17. Shang, J. S.; and Hankey, W. L., Jr.: Numerical Solution of the Navier-Stokes Equations for Supersonic Turbulent Flow Over a Compression Ramp. AIAA Paper No. 75-3, Jan. 1975.

18. Werle, M. J.; and Bertke, S. D.: Application of an Interacting Boundary Layer Model to the Supersonic Turbulent Separation Problem. Report No. AFL 76-4-21. Department of Aerospace Engineering. University of Cincinnati, Cincinnati, Ohio, 1976.

19. Nakayama, A.; Patel, V. C.; and Landweber, L.: Flow Interaction Near the Tail of a Body of Revolution. Part 2: Iterative Solution for Flow Within and Exterior to Boundary Layer and Wake. ASME, Journal of Fluids Engineering, Sept. 1976.

20. Davis, R. T.: Numerical and Approximate Solution of the High Reynolds Number Small Separation Problem. Vol. IV - Conference Proceedings for Advances in Engineering Science. NASA CP-2001, 1976, pp. 1451-1465.

21. Mathlab Group: MACSYMA Reference Manual. Project MAC, Mass. Inst. of Tech., Cambridge, Mass., 1975.

ORIGINAL PAGE IS
OF POOR QUALITY

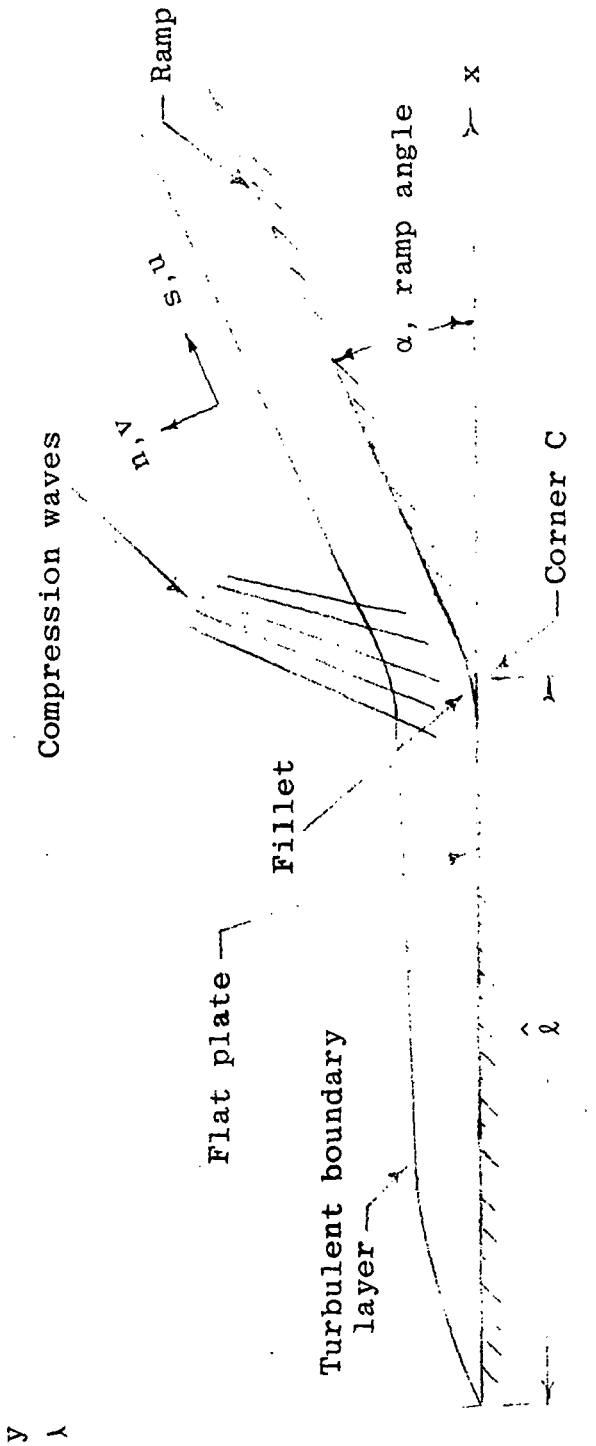

Figure 1.- Theoretical model.

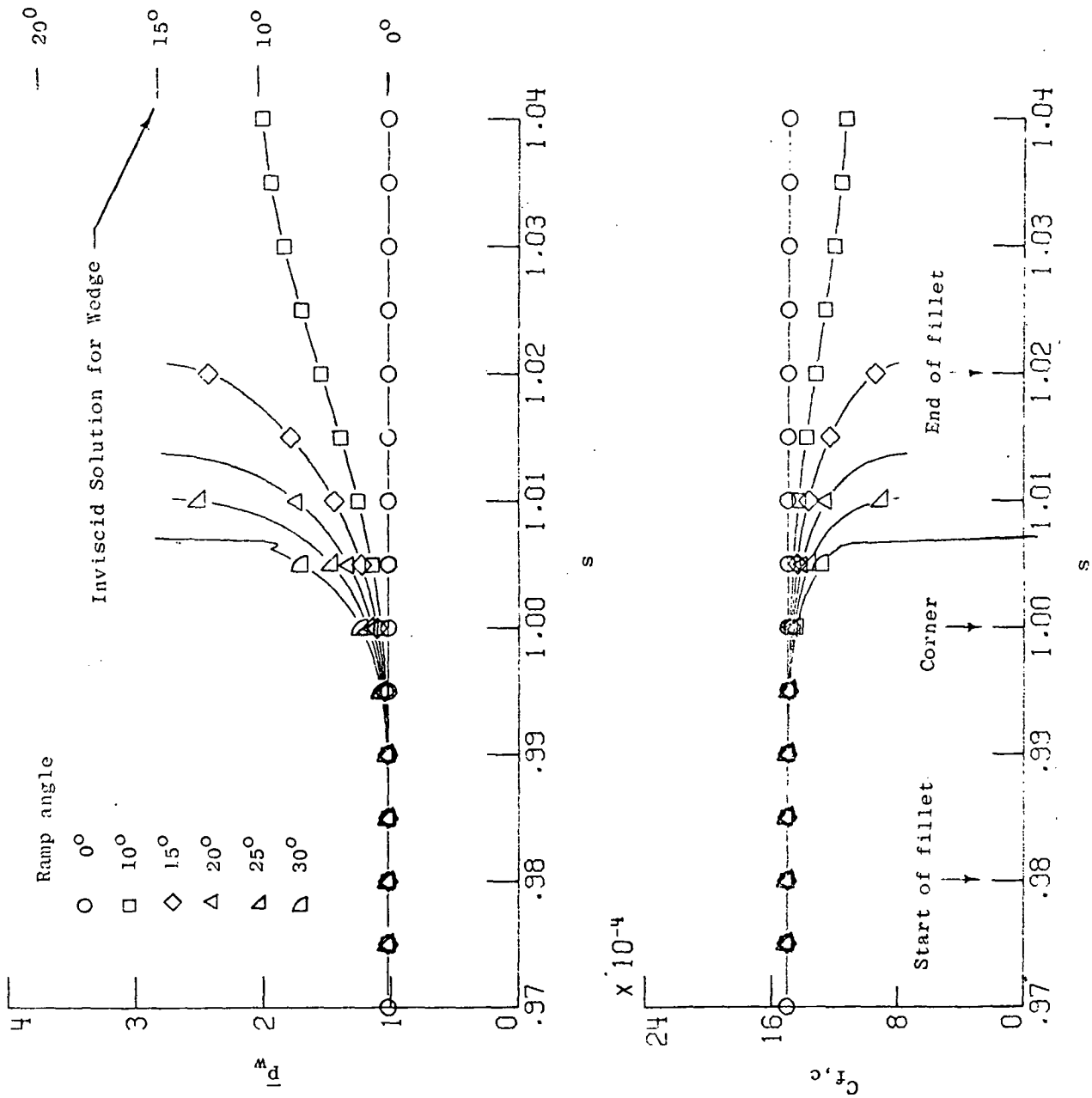

Figure 2.- Effect of ramp angle. D = 0.02

ORIGINAL PAGE IS
OF POOR QUALITY

ORIGINAL PAGE IS
OF POOR QUALITY

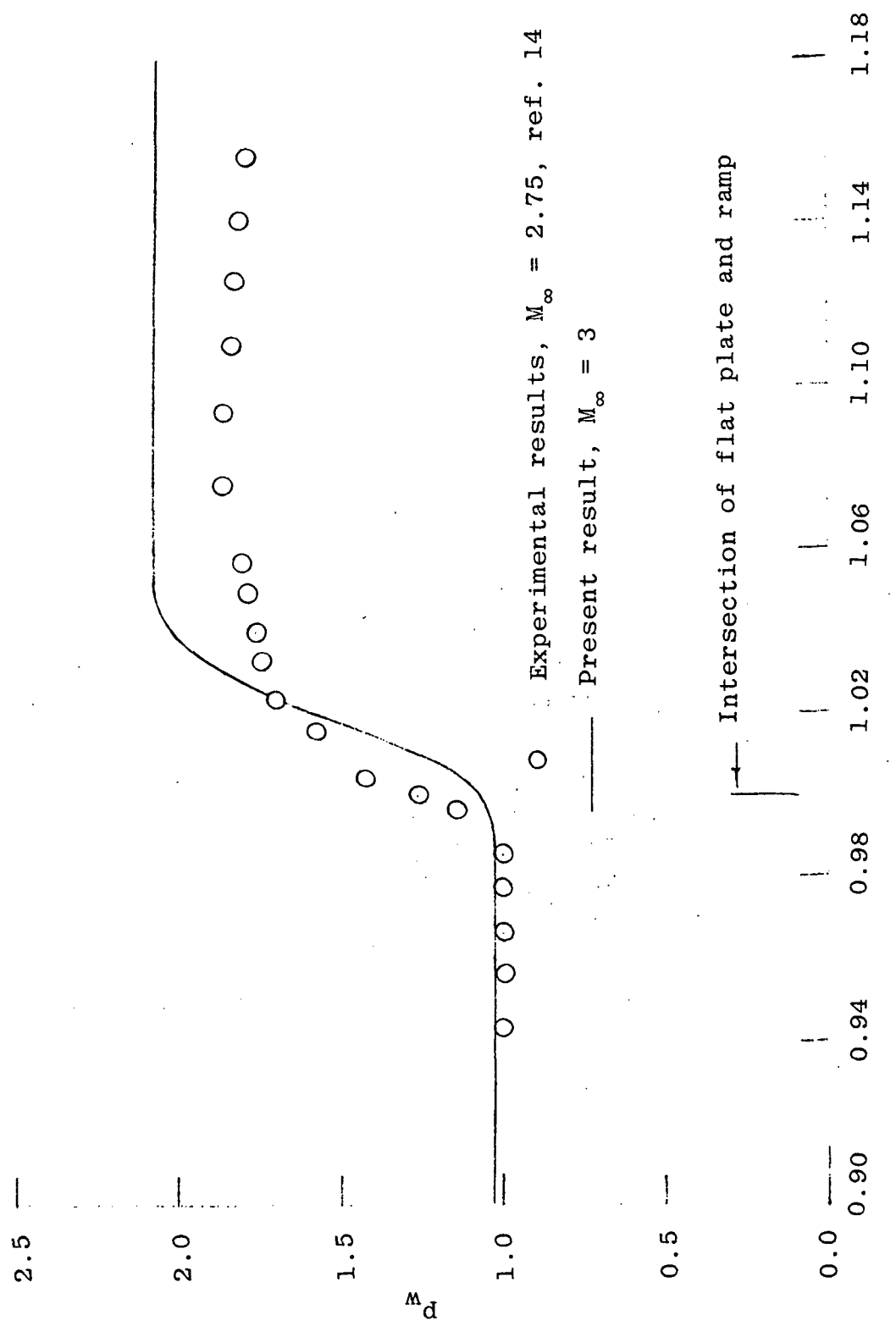

Figure 3.- Comparison of calculated pressure distribution with experimental results. $\alpha = 10^o$, D = 0.02, R_∞ (present calculations = $10X10^6$, R_∞ (experiment) = $2.1X10^6$.

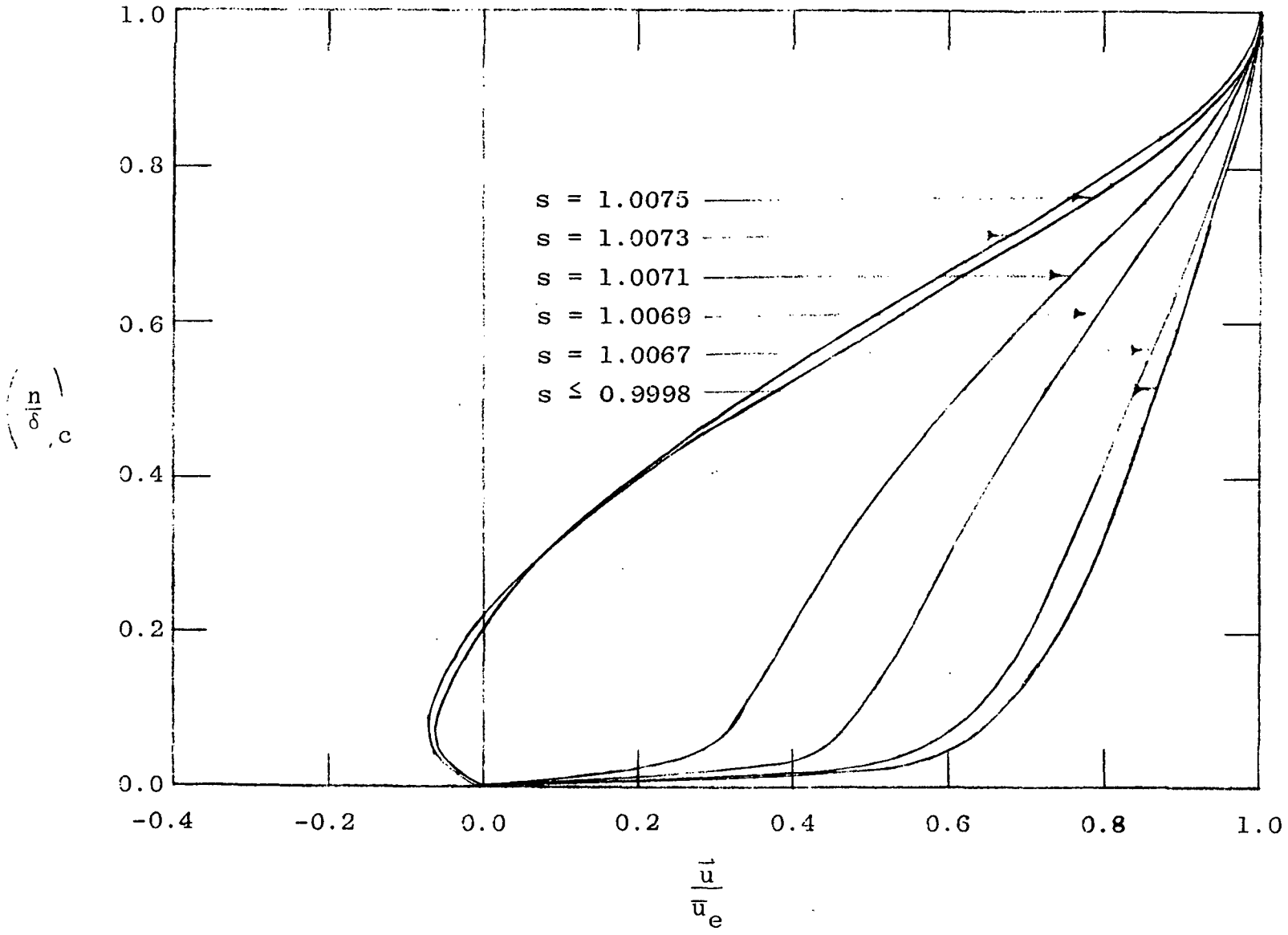

Figure 4.- Typical velocity profiles. D = 0.02, $\alpha = 30^{o}$

ORIGINAL PAGE IS
OF POOR QUALITY

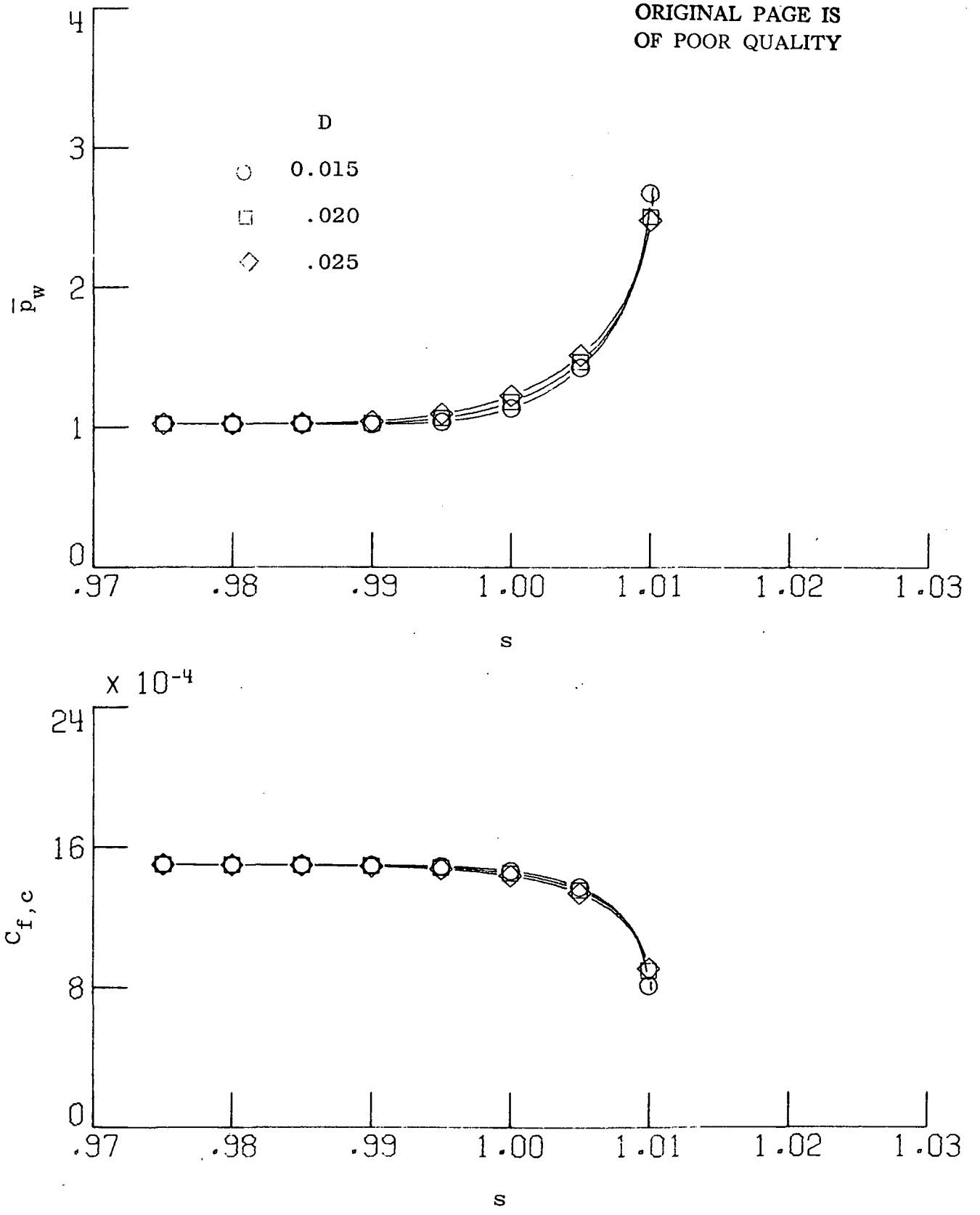

Figure 5.- Effect of fillet length. $\alpha = 25^{o}$

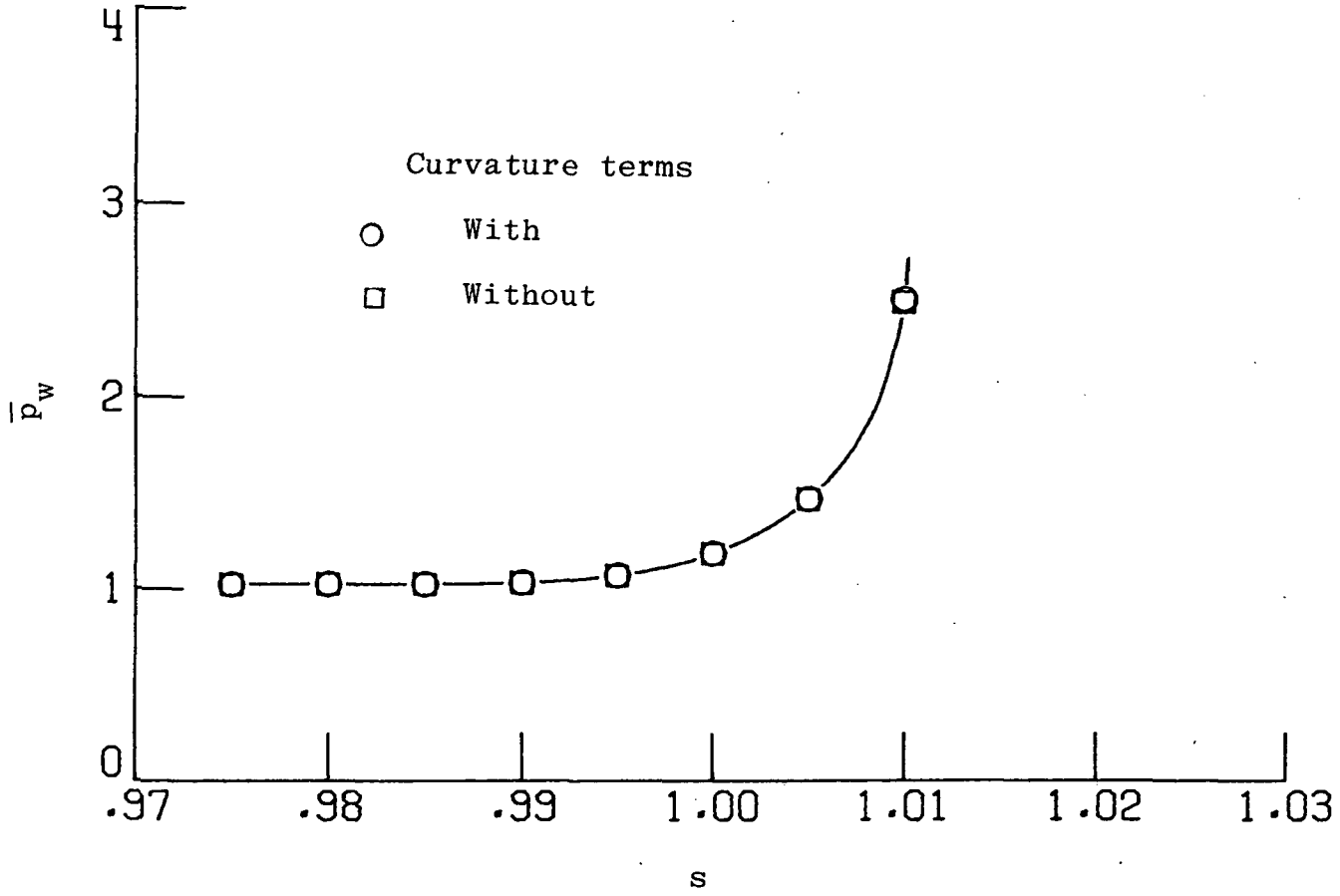

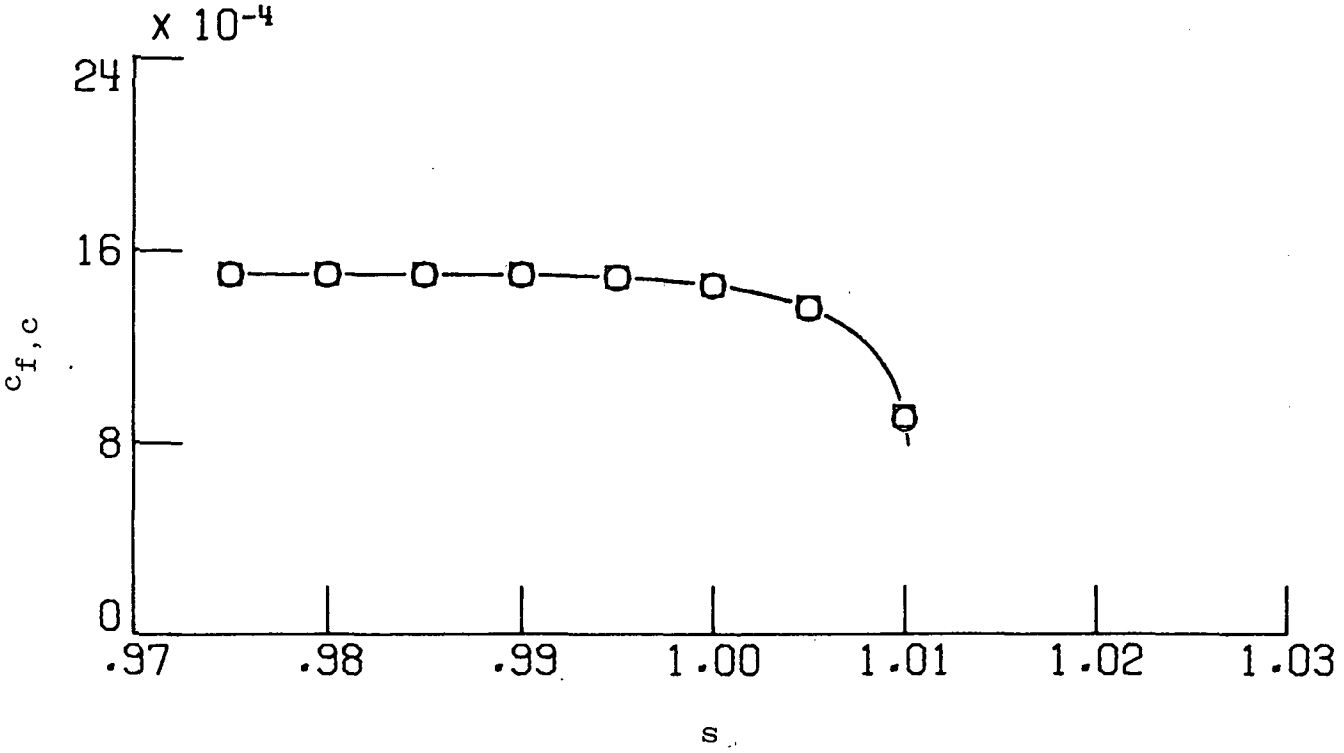

Figure 6.- Effect of curvature terms. D = 0.02; $\alpha = 25^{\circ}$

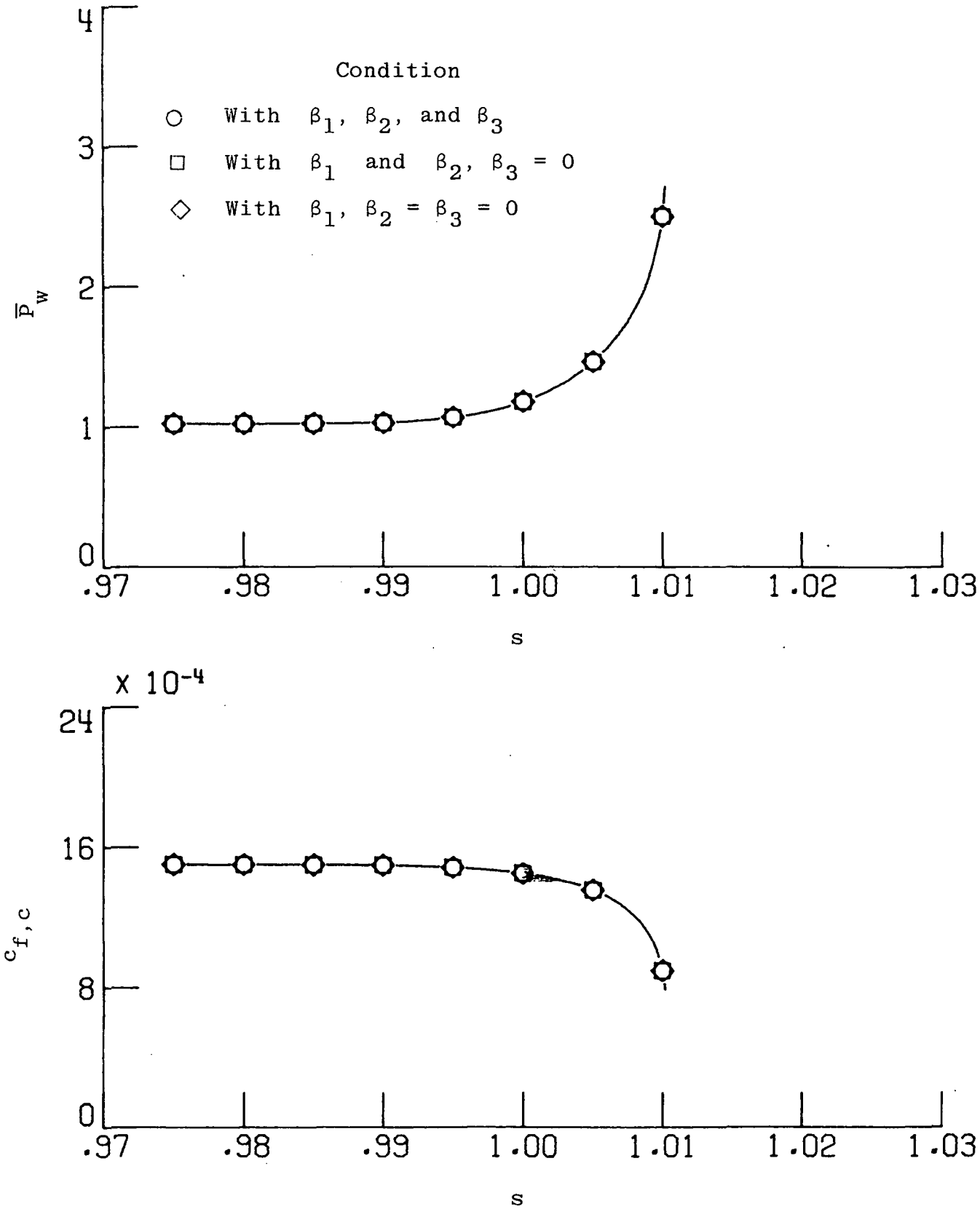

Figure 7.- Effect of eddy-viscosity parameters. D = 0.02; $\alpha = 25^{\circ}$

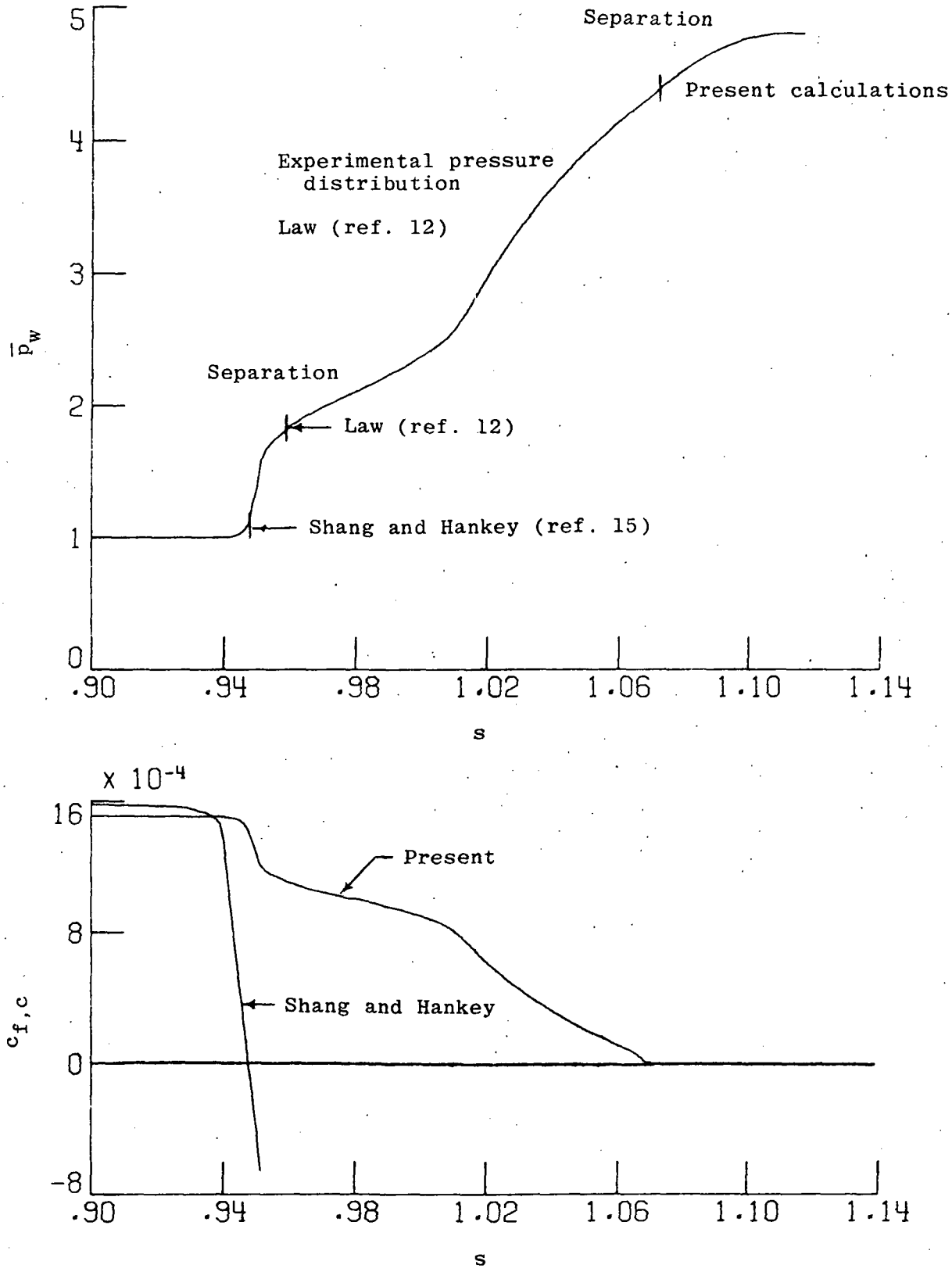

Figure 8.- Comparison of separation point from present calculations with those derived from Law and Shang and Hankey. $M_\infty = 3.0$; $D = 0.02$, $\alpha = 25^\circ$.

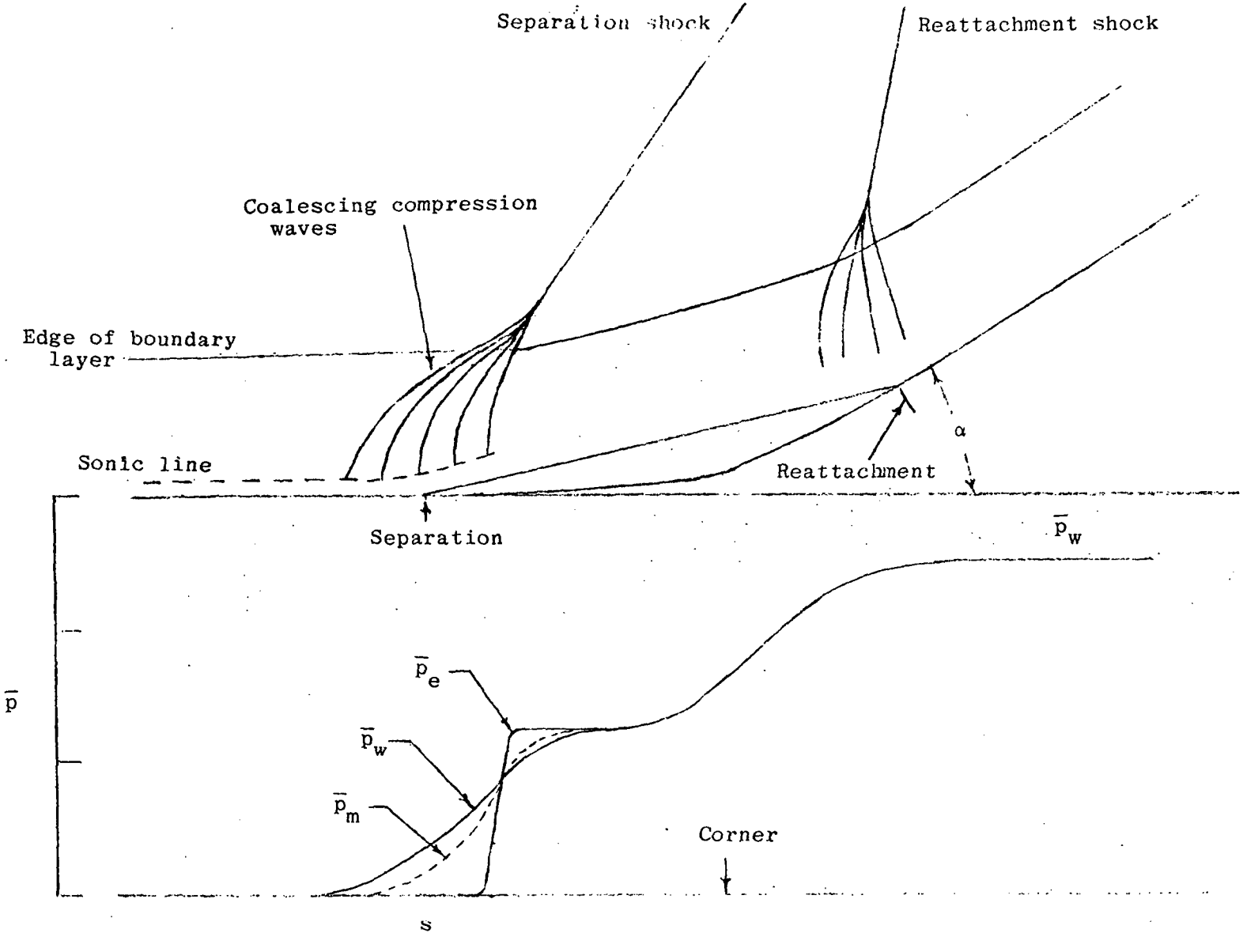

Figure 9.- Effects of coalescing compression waves on mean adverse pressure gradient under separation shock.

ORIGINAL PAGE IS OF POOR QUALITY

Figure 10.- Design of fillets. Fillet and angle in sketch correspond to fillet designed by 9th power polynomial with D = 0.02 and α = 30°

ORIGINAL PAGE IS
OF POOR QUALITY

ORIGINAL PAGE IS
OF POOR QUALITY

1. Report No.	2. Government Accession No.	3. Recipient's Catalog No.
NASA TM 74065		

4. Title and Subtitle	5. Report Date
Investigation of Supersonic Turbulent Boundary-Layer Separation on a Compression Ramp by an Integral Method Method	October 1977
	6. Performing Organization Code
7. Author(s)	8. Performing Organization Report No.
D. K. Patel and K. R. Czarnecki	
9. Performing Organization Name and Address	10. Work Unit No.
NASA Langley Research Center Hampton, Virginia 23665	505-06-11-02
	11. Contract or Grant No.
	13. Type of Report and Period Covered
12. Sponsoring Agency Name and Address	NASA Technical Memorandum
National Aeronautics and Space Administration Washington, DC 20546	14. Sponsoring Agency Code

15. Supplementary Notes

D. K. Patel - NRC Research Associate now with E.G.&G. Idaho, Inc.

16. Abstract

An investigation was made to determine the feasibility of using a boundary-layer integral method to study the separation of a turbulent boundary layer on a two-dimensional ramp at supersonic speeds. The numerical calculations were made for a free-stream Mach number of 3, a Reynolds number of 10 million, and over a ramp angle range from 0° to 30°. The investigation indicated a major deficiency in the approach which prevented the numerical calculations from being in good agreement with experiment or with those calculated by time-dependent Navier-Stokes methods.

17. Key Words (Suggested by Author(s)) (STAR category underlined)	18. Distribution Statement
Fluid Mechanics Boundary Layer - Turbulent Flow Separation Integral Method	Unclassified-Unlimited

19. Security Classif. (of this report)	20. Security Classif. (of this page)	21. No. of Pages	22. Price*
Unclassified	Unclassified	60	$4.50

*Available from The National Technical Information Service, Springfield, Virginia 22161